Memoirs of the Faculty of Engineering, Nagoya University
Vol. 37, No. 1 (1985)

FRICTIONAL PROPERTIES OF A SURFACE COVERED WITH A SOFT METAL FILM

SHINOBU KATO, ETSUO MARUI*
and KIYOO TACHI**

Department of Electronic-Mechanical Engineering

(Received May 20, 1985)

Abstract

It is known that the frictional properties of surfaces covered with soft metal film differ from those between surfaces without films. The aim of the present study is to clarify the effect of surface films on the frictional properties. First, the frictional properties in contact between a single hard protuberance and a surface electroplated with a film of soft metal are investigated experimentally and theoretically. As a result, a simple empirical expression of friction which represents the effect of the surface film and the load dependency is presented. And the plane strain deformation model of the soft metal film is offered in the analysis. Next, the interference effect of the film deformation between protuberances on the frictional properties is discussed in the contact of an indentor having two spherical protuberances located closely, to obtain a basic knowledge for the investigation of real engineering surfaces.

CONTENTS

* Department of Mechanical Engineering, Gifu Univesity
** Department of Mechanical Engineering, Toyama National College of Technology

1. Introduction

In many cases, direct contact of metals is usually prevented by a soft thin surface film that is different from bulk materials.

It has been shown that the frictional properties of surfaces covered with soft metal film differ from those between surfaces without films. Although it is known that the frictional coefficient is almost constant regardless of the vertical load in ordinary contact of surfaces without films, a load dependency of friction has been found in the friction of surfaces covered with soft surface films[1~5]. Figure 1 shows experimental examples of the coefficient of friction obtained by Tsuya and Takagi[2], which were obtained in an experiment on two cylindrical specimens having annular sliding surfaces with a lead-coated upper specimen and an electro-polished lower one. The substrate metal was copper. In the figure, the coefficient of friction decreases with the increase of load when the surface is

covered with a soft thin film. Bowers and Zisman[3] and Finkin[4] obtained the coefficient of friction of surfaces covered by soft thin films as a function of applied load, using the elastic deformation theory. Rabinowicz[5] showed that the coefficient of friction is affected by the surface film thickness and obtained the coefficient of friction as a function of film thickness theoretically. However, the mechanism and properties of the friction characteristics have not yet been sufficiently clarified.

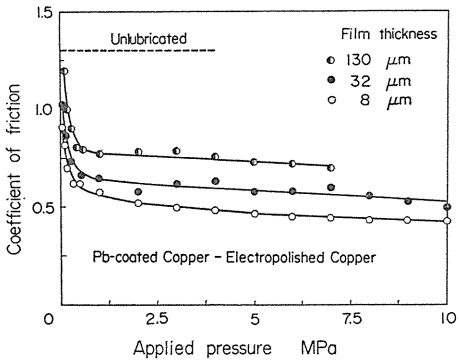

Fig. 1. Coefficient of friction vs. applied pressure for various lead film thickness [Tsuya and Takagi].

The aim of the present study is to clarify the effect of surface films on the frictional properties. In Chapter 2 of this research project, the frictional properties in contact between a single hard protuberance and a surface electroplated with a film of soft metal are investigated experimentally. The protuberance used in the experiment is a hard steel ball, because the shape of micro asperities on many real engineering surfaces may be regarded as spherical in analyzing a contact problem[6], and a spherical model experiment is convenient in the estimation of friction properties between real engineering surfaces with thin surface film. A simple empirical expression of friction which represents the effect of the surface film properties is then presented.

In Chapter 3, an analytical investigation of friction is undertaken theoretically. The coefficient of friction is calculated on the basis of the proposed plane strain plasticity model of the deformation of the surface film under the leading face of a spherical protuberance, in order to clarify the effects of the surface film on the friction characteristic, and to ascertain the mechanism of the load dependency of friction observed in Chapter 2.

A real engineering surface is composed of many accumulated micro asperities. The investigation of friction properties between such an engineering surface covered with soft metal film is an important practical problem. The interference effect may be induced by a plastic flow of soft metal film put between two adjacent micro asperities. The friction properties of such a case are considered to be greatly influenced by this interference.

In Chapter 4, the interference effect on the frictional properties is discussed, in the case of contact of an indentor having two model spherical protuberances located closely and a soft metal film, to obtain a basic knowledge for the investigation of real engineering surfaces.

2. Experiment of Friction between Single Spherical Protuberabce and Surface Covered with Soft Thin Film[7]

2. 1. Experiment of friction

2. 1. 1. Experimental apparatus and method

In the experiment, a steel ball is used as a single protuberance, which is pressed against the electroplated surface of a rotating disc to measure the frictional force as shown in Fig. 2. The apparatus used is shown in Fig. 3.

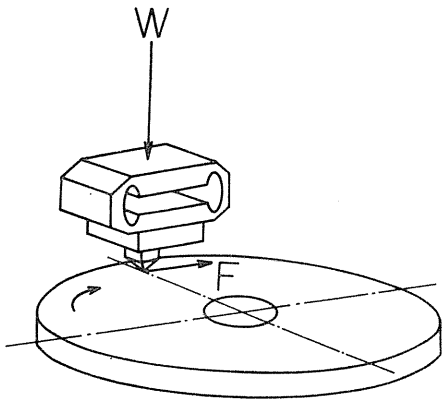

Fig. 2. Sketch of single protuberance slider on flat soft metal film.

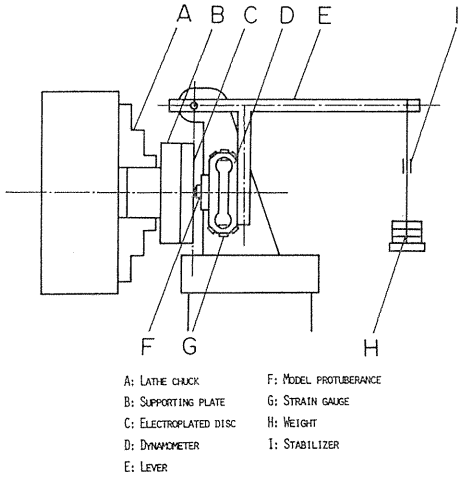

Fig. 3. Experimental apparatus.

An electroplated disc C is attached to the chuck of a lathe and rotated at a constant speed. The steel ball fixed in a holder F is pressed against the electroplated surface of the rotating disc, and two components of the force acting on the ball are measured. The measuring device is an annular dynamometer D, which is connected to the lever E, and load is applied by the weight H. In this case, the loading apparatus is installed so that the line of frictional force just passes through the fulcrum of the lever E, causing the force exerted by the lever to act vertically on the disc surface. The annular dynamometer D has been widely employed as a cutting force dynamometer[8] in measuring the two components of cutting force. It can measure simultaneously the vertical and tangential components of force acting on the steel ball by the two sets of strain gauges G.

It is found from the calibration of the dynamometer that the relations between the two components of force and the gauge strains showed a good linearity, and the amount of mutual interference is within 2 %.

The disc material is S35C (0. 35 % carbon steel). Two kinds of surface film are used to clarify the effect of surface film property. The surface of the disc is ground (surface roughness is 0. 5~0. 8 μm Rmax) and then electroplated by Pb or Pb-Sn-Cu as shown in Table 1. A boronfluoride bath alloy plating method is used

Table 1 Soft metal surface film

Metal electroplated (%)	Vickers hardness MPa
Pb(100)	100
Pb(87.8)-Sn(10.1)-Cu(2.1)*	200

* Pb-alloy

in plating. The film thickness are estimated from the difference of the height between plated and non-plated surfaces, which are measured by a roughness meter. Micro-Vickers hardness of the electroplated film is measured under very light load and shown in the same table. Since hardness is influenced by substrate, the listed values may not represent the exact hardness of the film, but are useful indications as to the hardness. The diameters of the steel balls are 1.00, 1.98, 3.18 and 3.97 mm, and rubbing speed is 2 cm/sec. The steel ball surface is always cleaned with trichloroethylene prior to sliding test, and all experiments are carried out at room temperature. An example of recorded oscillogram of the applied load W and frictional force F is shown in Fig. 4.

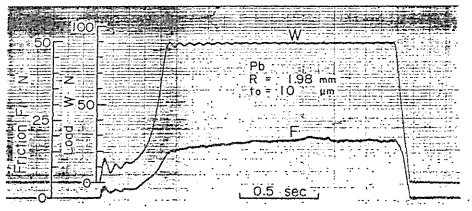

Fig. 4. Experimental record of applied load W and friction force F.

2. 1. 2. Experimental results

The general relation between applied load W and coefficient of friction μ obtained experimentally is shown in Fig. 5 for Pb-electroplated metal film. Coefficient of friction μ decreases considerably with the increase of applied load W in the small load range. Moreover, at a critical load, the electroplated surface film is ruptured, and the direct contact of spherical protuberance and substrate metal begins. Thereafter, coefficient of friction μ increases slowly with the applied load W. In the later part of this research, the effect of surface film on the friction is discussed in the small load ($W<W_c$: critical load) where the surface film does not rupture.

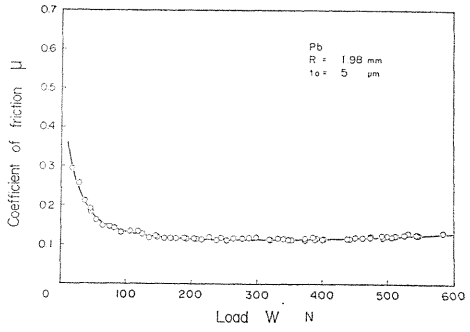

Fig. 5. Relation between coefficient of friction μ and load W (Pb-electroplated film, sphere radius 1.98 mm).

Figures 6, 7 show the variation of coefficient of friction for Pb- and Pb-Sn-Cu-electroplated metals, in the small load range. The lines in these figures represent the values for the coefficient of friction as calculated by the empirical

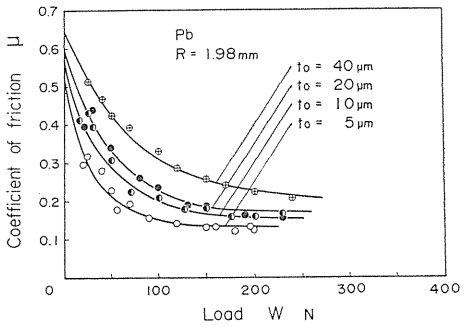

(a) Sphere radius 1.98 mm.

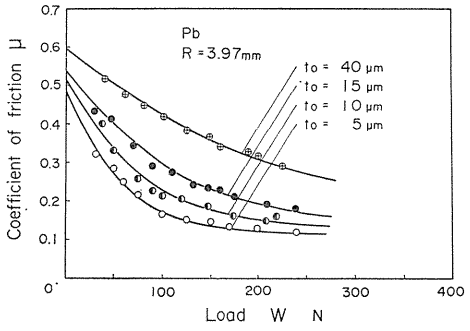

(b) Sphere radius 3.18 mm.

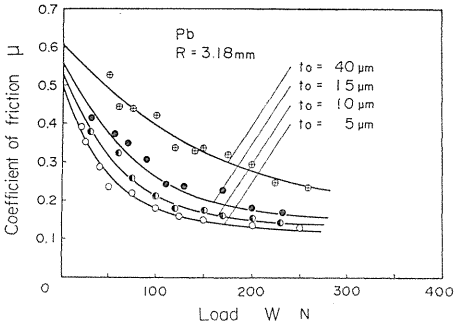

(c) Sphere radius 3.97 mm.

Fig. 6. Relation between coefficient of friction μ and load W (Pb-electroplated film, parameter is film thickness t_0).

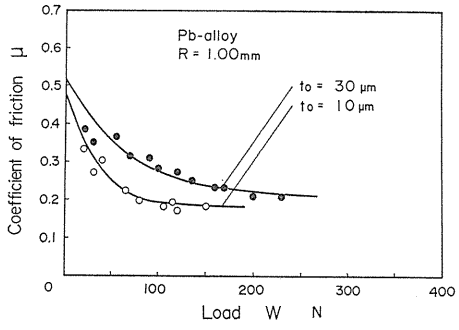

(a) Sphere radius 1.00 mm.

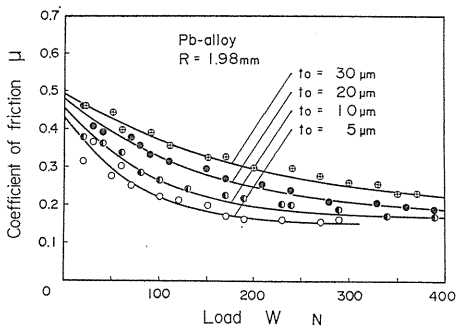

(b) Sphere radius 1.98 mm.

Fig. 7. Relation between coefficient of friction μ and load W (Pb-Sn-Cu-electroplated film, parameter is film thickness t_0).

expression indicated by equation (8). From these experimental results, it can be recognized that the coefficient of friction does not obey Coulomb's law, but depends on the load. That is, the coefficient of friction decreases considerably with the increase in load. In general, the less the film thickness t_0 is, the smaller the coefficient of friction μ is. Also, it can be recognized that the decreasing characteristics are influenced seriously by the film materials, its thickness t_0 and the protuberance radius R.

2. 2. Simple empirical formula of coefficient of friction

It will be convenient in the practical problem of the contact between surfaces with many protuberances, that is, micro-asperities, if we have an empirical formula of coefficient of friction which represents the influences of various properties of the film and load dependency of the friction.

From the experimental results of Figs. 6 and 7, the relation between μ and W can be expressed as follows:

$$\mu=\mu_2+(\mu_1-\mu_2)e^{-f(W)} \tag{1}$$

In this equation, μ_2 is the minimum coefficient of friction where the critical load is applied and the surface film is just ruptured, when the penetration depth of the protuberance is equal to the film thickness t_0. And μ_1 is the coefficient of friction extrapolated to the case in which $W=0$. The example expression of equation (1) is Fig. 8.

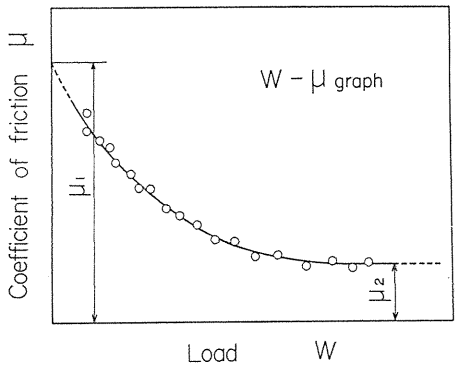

Fig. 8. Arrangement of experimental $\mu-W$ relation.

The function $f(W)$ represents the load dependency of the coefficient of friction and must satisfy the following conditions, to be in conformity with the fact that $\mu=\mu_1$ when $W=0$ and $\mu=\mu_2$ when W becomes sufficiently large:

(A) $f(W)=0$ when $W=0$, and

(B) $f(W)=\infty$ when W approaches infinity.

First, the expression of μ_2 is examined. The coefficient of friction at the critical load is influenced by the shearing and the ploughing of the surface film. Tsukizoe and Hisakado[9] analyzed the contact problem of spherical protuberance and soft metal surface and obtained the following expression of coefficient of friction.

$$\mu=\frac{\frac{4}{3\pi}\varphi+\mu_0}{1-\frac{4}{3\pi}\mu_0\varphi} \tag{2}$$

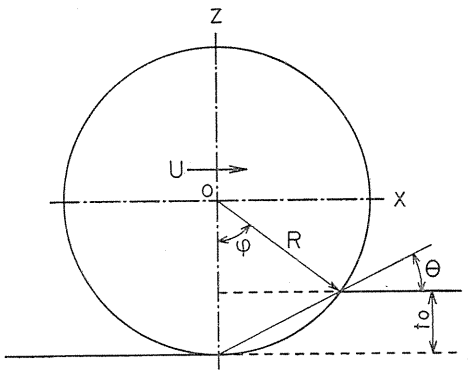

Fig. 9. Contact angle.

where φ is the angle shown in Fig. 9, which represents the penetration depth, and μ_0 is the shearing coefficient of friction. When the penetration depth t_0 is small as compared with the radius of protuberance, angle φ is considered to be very small and equation (2) is approximated as follows:

$$\left.\begin{aligned}\mu&=\mu_0\left(1+\frac{4}{3\pi\mu_0}\varphi+\frac{4\mu_0}{3\pi}\varphi+\frac{19}{9\pi^2}\varphi^2\right)\\ \text{where}\quad\varphi&=\sqrt{\frac{2t_0}{R}}\end{aligned}\right\}\qquad(2)'$$

This equation indicates that coefficient of friction μ is the function of the shearing coefficient of friction μ_0 and the angle φ, that is, $\sqrt{t_0/R}$.

Considering this result, the coefficient of friction μ_2 obtained from the experimental results of Figs. 6, 7 and so on are plotted against $\sqrt{t_0/R}$, that is, contact angle θ $(=\sqrt{t_0/2R})$ in Fig. 9. The angle θ is the measure of the film deformation in contact. The result is shown in Fig. 10, for Pb- and Pb-Sn-Cu-electroplated films. The plotted points of μ_2 lie on a smooth curve determined for each surface film. The yield pressure of Pb-Sn-Cu-film is larger than that of Pb-film, and the ploughing effect may be remarkable in Pb-Sn-Cu-film. Thus, the value of μ_2 is larger for Pb-Sn-Cu-film than for Pb-film. $\sqrt{t_0/R}$ may be assumed as follows:

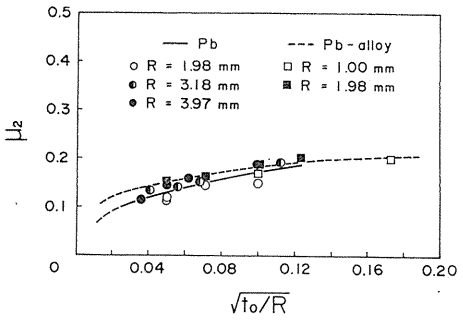

Fig. 10. Relation between minimum coefficient of friction μ_2 and $\sqrt{t_0/R}$.

The functional relation between μ_2 and

$$\mu_2=\mu_{20}\left\{1+\beta\left(\sqrt{\frac{t_0}{R}}\right)^n\right\}\qquad(3)$$

where coefficient β and index number n represent the ploughing effect of surface film and determined by the properties of the surface film. When the surface is covered with a film of infinitely small thickness and this is just ruptured, the coefficinet of friction is μ_{20}. In this case, the pressure generated in the film may be approximately equal to the yield pressure of the substrate metal, but the shearing strength is that of the film. Hence, μ_{20} can be written as follows:

$$\mu_{20}=\frac{k_f}{p_s}\qquad(4)$$

where k_f is the shearing strength of the film and p_s is the yield pressure of the substrate metal.

Values of μ_2 calculated by equation (3) are shown in Fig. 10, using parameter values shown in Table 2 for each film material. The experimental values of μ_2 agree well with the calculated ones.

Next, μ_1 is the coefficient of friction at the extreme condition in which $W=0$. This coefficient of friction may be determined by the film propeties which can be affected by the substrate metal. As the precise measurement of μ_1 at the extremely small load is impossible, the experimental value of μ_1 is estimated by the technique herewith described.

Table 2 Characteristic values included in empirical expression of coefficient of friction

Metals electroplated	μ_{10}	μ_{20}	α	β	m	n	b*	δ
Pb	0.0289	0.0289	31.4	15.6	0.205	0.498	2.35	1.07
Pb-Sn-Cu	0.0514	0.0514	12.1	6.3	0.165	0.398	1.32	1.07

$*b=\gamma/\sqrt{t_0/R}$

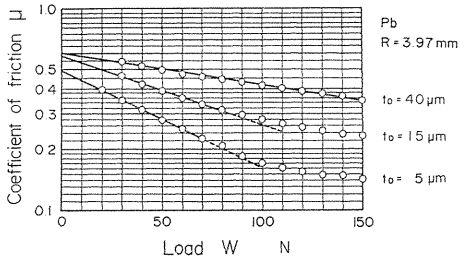

Fig. 11. Relation between coefficient of friction μ and load W (semi-log plotting).

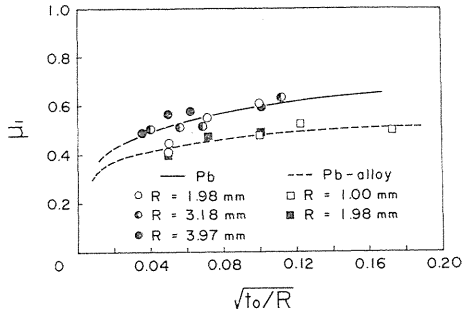

Fig. 12. Relation between coefficient of friction μ_1 when $W=0$ and $\sqrt{t_0/R}$.

The experimental relation between μ and W is again plotted on a semi-log paper as shown in Fig. 11. A linear relationship between μ and W is recognized in the small load region. The thicker the surface film t_0 is, the wider the linear portion becomes, and μ_1 is obtained as an interescting point of μ-axis and the extrapolated linear relationship. The coefficient of friction μ_1 obtained for various film thickness t_0 and protuberance radii R is plotted against $\sqrt{t_0/R}$, as in the former case of the minimum coefficient of friction μ_2 of Fig. 10. The result is shown in Fig. 12. The plotted points of μ_1 exist on a smooth curve determined for each surface film. Thus, the coefficient of friction μ_1 is uniquely determined by the value of $\sqrt{t_0/R}$ for each film material. Accordingly, the film properties, which may be affected by the substrate metal, is approximately estimated by the value of $\sqrt{t_0/R}$, for each film material. It is recognized in Fig. 12 that the coefficient of friction μ_1 for Pb-Sn-Cu-film, which is the harder one, is smaller than that for Pb-film, which is the softer one. The reason for this may be as follows: The relative properties of surface film which are determined in the combination of the film and the substrate, that is, the effects of the substrate metal on film properties are different from each other owing to the film hardness. The functional relation between μ_1 and $\sqrt{t_0/R}$ may be assumed, as in the case of μ_2, as follows:

$$\mu_1=\mu_{10}\left\{1+\alpha\left(\sqrt{\frac{t_0}{R}}\right)^m\right\} \tag{5}$$

where coefficient α and index number m represent the degree of effect of substrate metal on film properties. When the surface is covered with a film of infinitely

small thickness and the applied load W is infinitely small, the coefficient of friction becomes μ_{10}. In this case, the pressure generated and the shearing strength are the same as those of μ_{20}. The value of μ_{10} can be obtained from the following relation.

$$\mu_{10}=\frac{k_f}{p_s} \tag{6}$$

Hence, both μ_{10} and μ_{20} are considered to be equal. Calculated values of μ_1 by equation (5) are shown in Fig. 12, using parameter values shown in Table 2 for each film material. The experimental values of μ_1 agree well with the calculated ones.

Lastly, the function $f(W)$ representing the load dependency of the coefficient of friction is examined. The function $f(W)$ must be nondimensional, because it is a power of the exponential function. Furthermore, considering the above-mentioned conditions (A) and (B), $f(W)$ is assumed as follows:

$$f(W)=\gamma\left(\frac{W}{\pi R t_0 p_f}\right)^{\delta} \tag{7}$$

where the denominator $\pi R t_0 p_f$ represents the load carrying capacity of surface film itself (p_f is the yield pressure of surface film), when the penetration depth of spherical protuberance is equal to the film thickness t_0. Coefficient γ and index number δ represent the degree of load dependency of the coefficient of friction, and can be obtained from the experimental results of Figs. 6, 7 and so on.

From the above discussion, the empirical formula for the coefficient of friction (1) may be arranged as follows:

$$\frac{\mu}{\mu_{20}}=1+\beta\left(\sqrt{\frac{t_0}{R}}\right)^n+\left\{\alpha\left(\sqrt{\frac{t_0}{R}}\right)^m-\beta\left(\sqrt{\frac{t_0}{R}}\right)^n\right\}\mathrm{e}^{-\gamma\left(\frac{W}{\pi R t_0 p_f}\right)^{\delta}} \tag{8}$$

The values of γ and δ are determined so as to make equation (8) accord with the experimental results as shown in Figs. 6 and 7. The results are plotted against $\sqrt{t_0/R}$ for two kinds of surface films, that is, Pb- and Pb-Sn-Cu-electroplated films in Figs. 13 and 14. The value of γ increases linearly with the increase of $\sqrt{t_0/R}$; γ becomes zero, and the load dependency of the friction disappears when $\sqrt{t_0/R}$ reaches zero, as seen in Fig. 13. In other words, the load dependency of the coefficient of friction may become remarkable in the case of large film thickness t_0 and small protuberance radius R. Furthermore, it is recognized in Fig. 13 that the value of γ is large and the load dependency of the coefficient of friction μ is remarkable, when the soft surface film of Pb, which has a smaller yield pressure p_f than Pb-Sn-Cu-electroplated film, is used, and the penetration of the protuberance is likely to become deep. The slope b of γ-$\sqrt{t_0/R}$ line is also shown in Table 2. This b indicates the extent of the load dependency of μ for each film material.

The value of δ is a constant which is slightly greater than unity, regardless of the surface film materials, within the wide range of $\sqrt{t_0/R}$ as seen in Fig. 14.

Calculated results of μ by equation (8) are shown in Figs. 6 and 7 and are compared with the experimental results for various film thickness t_0, protuberance radii R and film materials. Both the experimental and calculated results accord

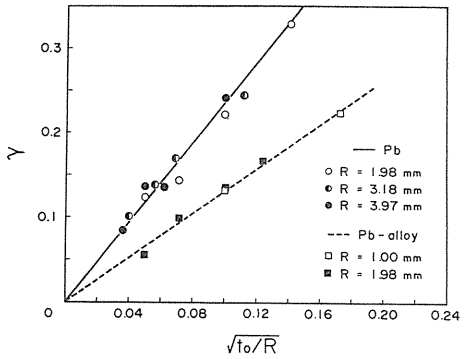

Fig. 13. Relation between coefficient γ and $\sqrt{t_0/R}$.

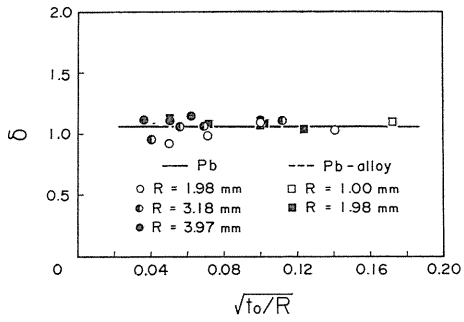

Fig. 14. Relation between index number δ and $\sqrt{t_0/R}$.

with each other within a wide range of applied load W, wherein the surface film does not rupture.

From the above discussion on empirical formulas, it is ascertained that the coefficient of friction μ can be precisely evaluated by equation (8), which is a function of the surface film, its thickness, protuberance radius and applied load, if the parameter values as shown in Table 2 are already obtained for a combination of the electroplated surface film and the substrate metal.

2. 3. Concluding remarks on experiment of friction between a single protuberance and surface

In the present study, various experiments are carried out using a steel ball as a protuberance in order to elucidate the properties of the friction of the surface covered by soft thin film. The load dependency of the coefficient of friction and effects of thickness and hardness of the film on the friction are clarified. The results obtained can be summarized as follows:

(1) In an experiment, the frictional properties of a surface covered with a soft thin metal film are clarified. It is recognized that the soft thin metam film is effective as a friction reducing agent in a light load condition.

(2) An empirical expression representing a load dependency of the coefficient of friction is introduced from experimental results as a function of various variables such as radius of a spherical protuberance, thickness and deformation resistance of soft metal films and so on.

(3) The load dependency of friction can be arranged uniquely by the value of $\sqrt{t_0/R}$ for a given film material. The greater the value of $\sqrt{t_0/R}$ is, the more remarkable the load dependency is.

3. Analysis of Friction between a Single Protuberance and Surface[10]

3. 1. Calculation of coefficient of friction based on a contact model between single spherical protuberance and surface

3. 1. 1. Deformation model of soft metal film

To clarify the mechanism of load dependency and the properties of friction, the coefficient of friction is analyzed theoretically in this chapter, by the herewith described deformation model of surface film.

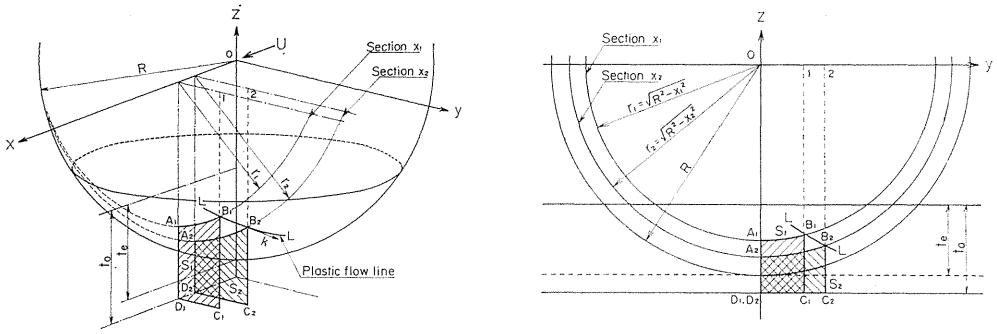

(a) General view. (b) Front view.

Fig. 15. Contact model of spherical protuberance and surface.

The force generated when the spherical protuberance penetrates the surface covered with soft film and is moved horizontally is calculated. Figure 15 shows the contact model of the spherical protuberance and surface. When the protuberance moves in the arrow direction, the surface film under the leading face of the spherical protuberance will be compressed between the leading face of the sphere and the underlying metal, and forced to flow out to both sides. Taking the center of the sphere as the origin, x-axis is determined in the direction of sphere movement, and z-axis is perpendicular to the contacting surface. Then, y-axis is determined in the direction of side flow of the surface film, an orientation that is perpendicular to both x- and z-axes. At the cross-section x_1 perpendicular to the protuberance movement, a small volume S_1 dx of surface film $A_1B_1C_1D_1$, which is surrounded by the sphere and underlying metal, and whose cross-sectional area is S_1, compressed so as to flow out to both sides by the protuberance movement. Accordingly, the cross-section of the same volume S_1 dx is considered to be $A_2B_2C_2D_2$, whose cross-sectional area is S_2 at the cross-section x_2. The plastic flow line of surface film described on the sphere is the curve LL which passes through the points B_1 and B_2. A tangent of this flow line indicates the moving direction of surface film on the protuberance sphere. The equation for the plastic flow line can be obtained as follows, when the penetration of the sphere is t_e ($t_e<t_0$; t_0 is the film thickness) :

From the condition of volume conservation,

$$S_1dx=S_2dx$$

Thus, the cross-sectional area S_i is constant at each perpendicular cross-section and equal to S. Putting the coordinate of the point B_1 as (x_1, y_1, z_1),

$$S=y_1(R+t_0-t_e)+\int_0^{y_1} z\,dy$$

$$=y_1(R+t_0-t_e)-\frac{1}{2}\left\{y_1\sqrt{R^2-x_1{}^2-y_1{}^2}+(R^2-x_1{}^2)\sin^{-1}\frac{y_1}{\sqrt{R^2-x_1{}^2}}\right\}$$

Then, the equation of flow line LL is given as follows:

$$\left.\begin{aligned} &f=y(R+t_0-t_e)-\frac{1}{2}\left\{y\sqrt{R^2-x^2-y^2}+(R^2-x^2)\sin^{-1}\frac{y}{\sqrt{R^2-x^2}}\right\}-S=0\\ &g=x^2+y^2+z^2-R^2=0 \end{aligned}\right\} \quad (9)$$

The directional cosines of the tangent at a given point (x, y, z) on the plastic flow line are given as follows:

$$\left.\begin{aligned} l^*&=\frac{\Delta_x}{\sqrt{\Delta_x^2+\Delta_y^2+\Delta_z^2}}\\ m^*&=\frac{\Delta_y}{\sqrt{\Delta_x^2+\Delta_y^2+\Delta_z^2}}\\ n^*&=\frac{\Delta_z}{\sqrt{\Delta_x^2+\Delta_y^2+\Delta_z^2}} \end{aligned}\right\} \quad (10)$$

where

$$\left.\begin{aligned} \Delta_x&=\begin{vmatrix}\frac{\partial f}{\partial y} & \frac{\partial f}{\partial z}\\ \frac{\partial g}{\partial y} & \frac{\partial g}{\partial z}\end{vmatrix}=2z(R+t_0-t_e-\sqrt{R^2-x^2-y^2})\\ \Delta_y&=\begin{vmatrix}\frac{\partial f}{\partial z} & \frac{\partial f}{\partial x}\\ \frac{\partial g}{\partial z} & \frac{\partial g}{\partial x}\end{vmatrix}=-2xz\sin^{-1}\frac{y}{\sqrt{R^2-x^2}}\\ \Delta_z&=\begin{vmatrix}\frac{\partial f}{\partial x} & \frac{\partial f}{\partial y}\\ \frac{\partial g}{\partial x} & \frac{\partial g}{\partial y}\end{vmatrix}=2xy\sin^{-1}\frac{y}{\sqrt{R^2-x^2}}-2x(R+t_0-t_e-\sqrt{R^2-x^2-y^2}) \end{aligned}\right\} \quad (11)$$

Considering that the shearing deformation stress k_f of the film acts along the plastic flow line, the x, y and z components of the shearing stress are represented by the following equations, respectively.

$$k_x=l^*k_f,\quad k_y=m^*k_f,\quad k_z=n^*k_f \quad (12)$$

In Fig. 15, the length of segment 12 equals $\sqrt{2Rt_e-t_e{}^2-x^2}$, and the average value $\bar{k}_y$ of the y component of the shearing stress k_y is represented by

$$k_y=\frac{k_f}{\sqrt{2Rt_e-t_e^2-x^2}}\int_0^{\sqrt{2Rt_e-t_e^2-x^2}} m^*dy \tag{13}$$

3. 1. 2. Yielding condition of soft metal film and contact pressre distribution

When the films are compressed under plane strain between upper and lower rigid surfaces as shown in Fig. 16, the pressure distribution p on the surface of the anvil can be obtained using the equations of equilibrium and yield condition[11]. Where the frictional shearing stress τ is acting on the surface, the equation of equilibrium in the y direction is

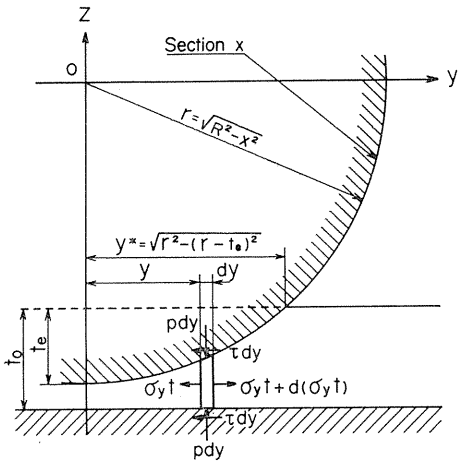

Fig. 16. Compression under plane strain.

$$\sigma_y t+2\tau dy=\sigma_y t+d(\sigma_y t)$$

And rearranging this equation,

$$\frac{d\sigma_y}{dy}=\frac{2\tau}{t}-\frac{\sigma_y}{t}\frac{dt}{dy} \tag{14}$$

where t represents the effective film thickness and is written as follows:

$$t=R+t_0-t_e-\sqrt{R^2-x^2-y^2} \tag{15}$$

The yield condition is

$$\sigma_y+p=2k_f \tag{16}$$

From the equations (14) and (16), it follows that

$$\frac{dp}{dy}+\frac{1}{t}\frac{dt}{dy}p=-\frac{2\tau}{t}+\frac{2k_f}{t}\frac{dt}{dy} \tag{17}$$

Assuming that $p=p_f$ at the point of $y^*=\sqrt{2Rt_e-t_e{}^2-x^2}$, where p_f corresponds to the deformation resistance (hardness) of the surface film, the pressure p is obtained by equation (17) as follows:

$$p=\frac{1}{t}\{2\tau(\sqrt{2Rt_e-t_e^2-x^2}-y)+2k_f(t-t_0)+p_ft_0\} \tag{18}$$

In this equation, we let $\tau=\bar{k}_y$ (a very rough assumption, but justified in practice if friction from calculation approximates the experimental value), and p does not exceed the deformation resistance p_s of the underlying metal; then, the pressure distribution can be obtained as follows:

$$\left.\begin{aligned} p&=\frac{1}{t}\{2\bar{k}_y(\sqrt{2Rt_e-t_e^2-x^2}-y)+2k_f(t-t_0)+p_ft_0\} \quad \text{in } p<p_s \\ p&=p_s \quad \text{in } p\geqq p_s \end{aligned}\right\} \tag{19}$$

3. 1. 3. *Calculation of coefficient of friction*

Now, in Fig. 17 showing the spherical protuberance, the area dA of spherical surface element 1234 is written as follows:

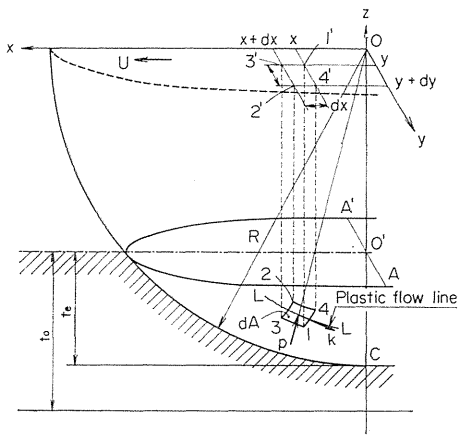

Fig. 17. Stress distribution on spherical protuberance.

$$dA=\frac{R}{\sqrt{R^2-x^2-y^2}}dx\,dy \tag{20}$$

Pressure p acts perpendicularly to this surface element, and shearing deformation stress of the film k_f acts along the flow line. The force components dF, dW in x and z directions acting on the small surface element 1234 are written as follows:

$$\left.\begin{aligned} dF&=(\bar{\lambda}p+l^*k_f)\,dA \\ dW&=(\bar{\nu}p+n^*k_f)\,dA \end{aligned}\right\} \tag{21}$$

where the directional cosines of the normal of the sphere are given by equation (22).

$$\bar{\lambda}=\frac{x}{R},\quad \bar{\mu}=\frac{y}{R},\quad \bar{\nu}=\frac{z}{R} \tag{22}$$

The frictional foce F and vertical force W can be represented as

$$F=2\int_0^{\sqrt{2Rt_e-t_e^2}}dx\int_0^{\sqrt{2Rt_e-t_e^2-x^2}}\frac{(\bar{\lambda}p+l^*k_f)R}{\sqrt{R^2-x^2-y^2}}dy \tag{23}$$

$$W=2\int_0^{\sqrt{2Rt_e-t_e^2}}dx\int_0^{\sqrt{2Rt_e-t_e^2-x^2}}\frac{(\bar{\nu}p+n^*k_f)R}{\sqrt{R^2-x^2-y^2}}dy \tag{24}$$

Therefore, the coefficient of friction μ can be obtained by

$$\mu=\frac{F}{W} \tag{25}$$

The calculation procedure of the coefficient of friction is as follows:

If the penetration depth $t_e(<t_0)$ is assumed, the directional cosines of the plastic flow line can be obtained by equations (10) and (11). Then, the pressure distribution on the protuberance is calculated by equations (13) and (19). In the next step, frictional force F and vertical force W are obtained by equations (23) and (24), as the directional cosines of the normal of the sphere surface are given in equation (22). After these calculations, the coefficient of friction is obtained by equation (25). As a result, the relation between coefficient of friction μ and vertical load W is clarified analytically.

In the calculation, the values of the deformation resistances of film and the substrate metal are determined by reference to the hardness test of Table 1 as follows:

p_s of the substrate metal = 2000 MPa
p_f of Pb-film = 100 MPa
p_f of Pb-Sn-Cu-film = 200 MPa

3. 2. Results of calculation and discussion

The coefficient of friction is obtained theoretically, and various investigations are made to ascertain the mechanism of film lubrication and the effects of the radius of spherical protuberance R, the thickness of the film t_0 and the deformation resistance p_f of the surface film, by obtaining a plastic flow line, pressure distribution under the leading face of the spherical protuberance and then calculating the load dependency of the coefficient of friction.

3. 2. 1. Plastic flow line and pressure distribution

The plastic flow lines and pressure distributions on the leading surface in the rubbing direction are shown in Fig. 18 for the case in which the point of protuberance does not yet penetrate through the surface film. In this figure, the origin O of the coordinate is shifted downwards to the point on sphere surface from the center of the sphere as shown in Fig. 15, to facilitate the understanding of the figure. Figs. (a)～(c) show the plastic flow lines on the sphere in each x-y, x-z, and y-z projection, where x-axis is parallel to the rubbing direction and z-axis is perpendicular to the surface. The plastic flow lines (e. g., line AB in the figures) near the x-axis run downwards (-z direction) along the spherical surface as seen in Fig. (b), fanning out somewhat in the width direction (y direction) as seen in Fig. (c). The plastic flow lines (e. g., line CD in the figures) more remote from x-axis run downwards at first and then curve upwards as seen in Fig. (b). There is a remarkable fanning out of the flow lines in y direction as seen in Fig. (c).

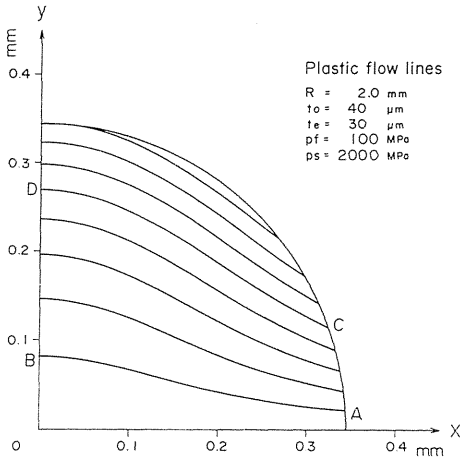

(a) $x-y$ projection of plastic flow lines.

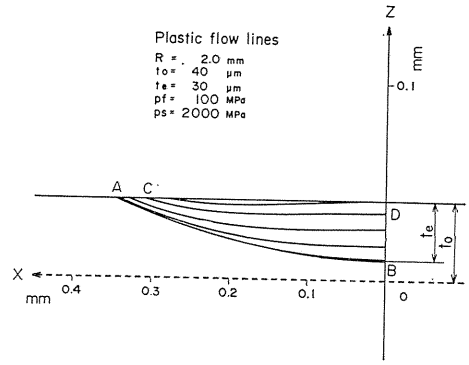

(b) $x-z$ projection of plastic flow lines.

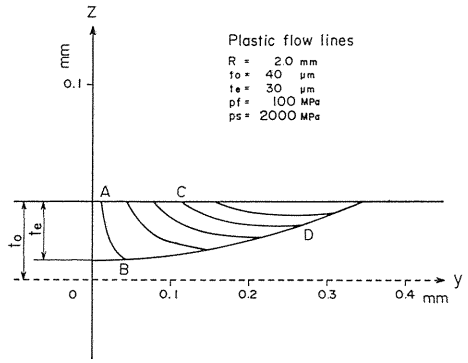

(c) $y-z$ projection of plastic flow lines.

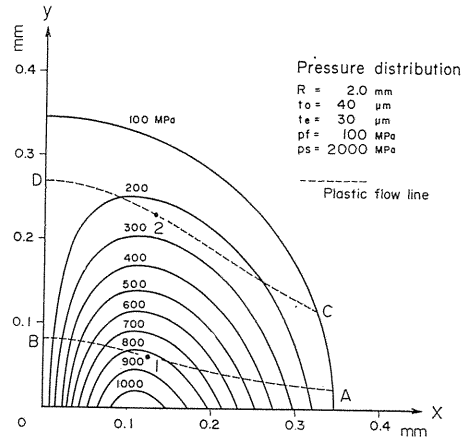

(d) Pressure distribution.

Fig. 18. Plastic flow lines and pressure distribution ($t_e < t_0$).

In view of these results, the density of the plastic flow lines on the spherical surface is greater in the x-y projection as the distance from the x-axis is greater.

Fig. (d) shows the pressure distribution. The distribution is symmetric about x-axis, and the distribution below x-axis is omitted in the figure. In the left side of y-axis, the contact between protuberance and surface film does ont occur and pressure is not generated. The pressure generated in the film is extremely high in comparison with the usual deformation resistance, i. e., hardness of the film. The pressure becomes maximum near the point $x=0.1$ mm on the x-axis. The pressure distribution corresponds well to the plastic flow lines. First, by comparing Figs. (a)~(d), and considering the pressure distribution along a given flow line (CD in the figure) that is distant from x-axis, the pressure rises along the plastic flow line as the flow line descends (C-2), and drops when it ascends (2-D). Next, in the case of plastic flow line AB in the figure, near x-axis, the pressure rises (A-1)

and then proceeds to drop (1-B) along a given plastic flow line; however, the plastic flow line runs consistently downwards near x-axis. This may due to the fact that the space between each plastic flow line is very large near y-axis. From these calculational results, it may be considered that the characteristic of pressure distribution near x-axis is mainly determined by the density of plastic flow lines in x-y (horizontal) plane and that of pressure distribution apart from x-axis is related to the density of plastic flow lines in x-z (vertical) plane.

Figure 19 shows the plastic flow lines and pressure distribution for the case in which the point of the protuberance just contacts the underlying metal. The fundamental properties of the plastic flow lines and pressure distribution are the same as those of Fig. 18. However, the next points are clear in Figs. (a)～(c), in which the fanning out of the plastic flow lines in y direction becomes remarkable and

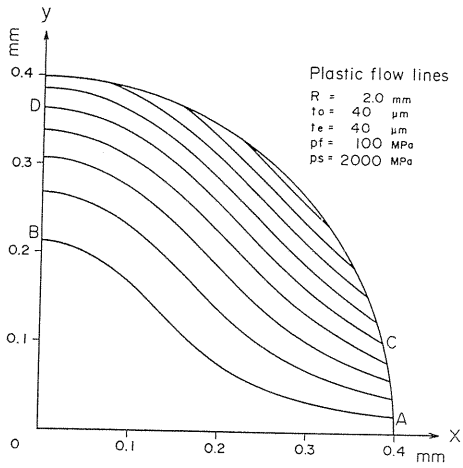

(a) $x-y$ projection of plastic flow lines.

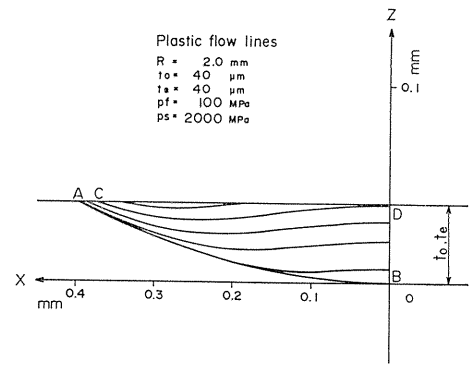

(b) $x-z$ projection of plastic flow lines.

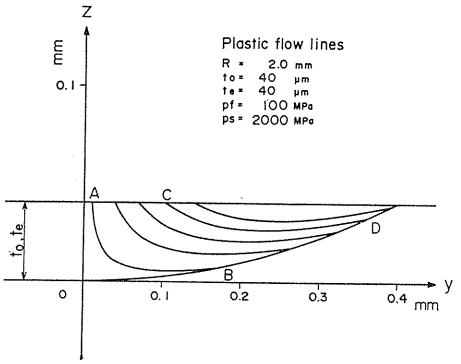

(c) $y-z$ projection of plastic flofw lines.

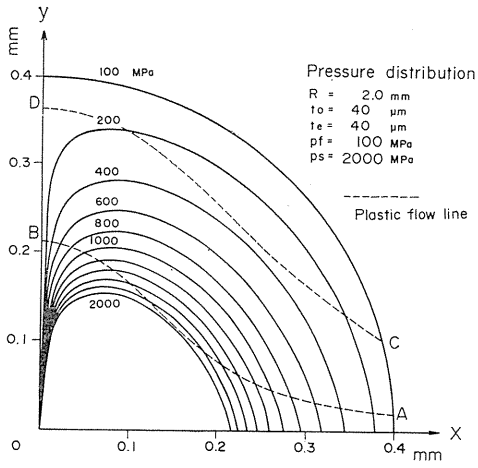

(d) Pressure distribution.

Fig. 19. Plastic low lines and pressure distribution ($t_e=t_0$).

the running direction of the plastic flow lines changes gradually from downwards to upwards, even in the plastic flow lines (e. g., AB in the figure) near x-axis. In Fig. (d), showing the pressure distribution, the pressure generated in the film reaches the deformation resistance of the underlying metal p_s over a fairly wide region, in terms of the increase in the protuberance penetration t_e.

3. 2. 2. Effects of surface film on coefficient of friction

As the coefficient of friction is considered to be influenced by the radius of the protuberance, the film thickness, deformation resistance and so on, the effects of these variables on the coefficient of friction are investigated. In the following calculation, $p_s=2000$ MPa and $k_s=p_s/\sqrt{3}$ are adopted, which correspond to the deformation resistance of S35C (0. 35%C carbon steel for machine structure).

(a) Effects of radius of spherical protuberance

Figure 20 shows the relation between the load and the coefficient of friction when the radius of spherical protuberance R is varied and the film thickness t_0 is kept constant. It is clear in the figure that the radius of protuberance R has a little effect on the coefficient of friction, and the coefficient of friction is slightly large in a large protuberance radius R. The reason for this may be considered as follows: In the large protuberance radius R, the penetration depth is shallow, and the restriction on film deformation exerted by the underlying metal is weak; hence, the pressure generated in the films is relatively low.

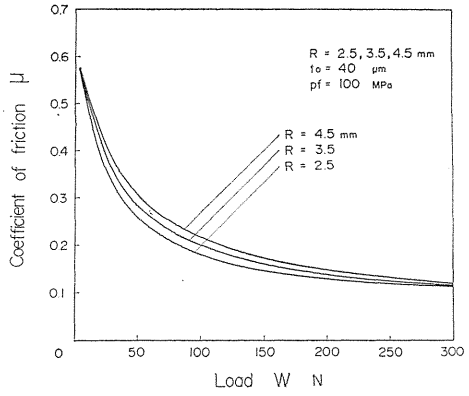

Fig. 20. Effect of radius of spherical protuberance R on coefficient of friction μ ($p_f=100$ MPa, $k_f=p_f/\sqrt{3}$).

The coefficients of friction are comparatively high under light load. This indicates that the protuberance contacts only the film and the deformation of the film is not affected by the underlying metal. When the load is increased, the deformation of the film is restricted by the underlying metal and high pressure is generated in the film, as seen in Figs. 18(d) and 19(d). As a result, the coefficient of friction rapidly decrease. In the load in which a low coefficient of friction is maintained, the surface film acts as a friction reducing agent between the underlying metal and the protuberance.

(b) Effects of surface film thickness t_0

Figure 21 shows the relation between the load and the coefficient of friction when the film thickness t_0 is varied and radius R is kept constant. From the results shown in the figure, it is clear that the thicker the film is, the larger the frictional load is and the more gradual the decrease of the coefficient of friction is. This fact may be explained by the restriction of the underlying metal and the ploughing effect of the surface film. Thus, in the case of a large film thickness, the restriction exerted by underlying metal and the pressure generated in the film are both relatively low, which makes the penetration depth great and the ploughing effect slightly large. As a result, the changing characteristic of coefficient of friction μ owing to load W in Fig. 21 may be obtained.

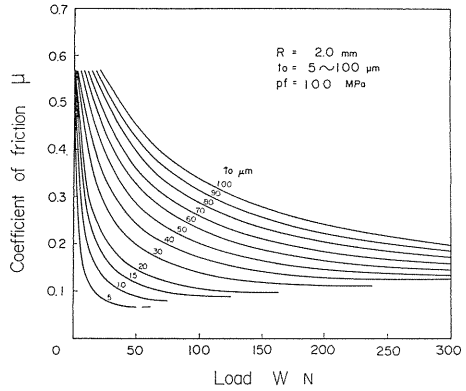

(a) p_f=100 MPa, R=2 mm.

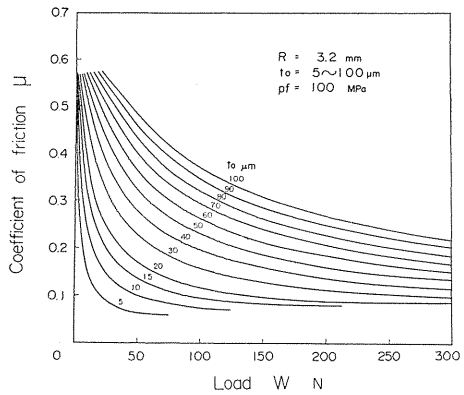

(b) p_f=100 MPa, R=3.2 mm.

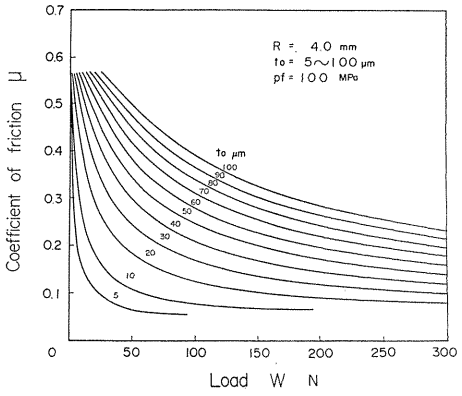

(c) p_f=100 MPa, R=4 mm.

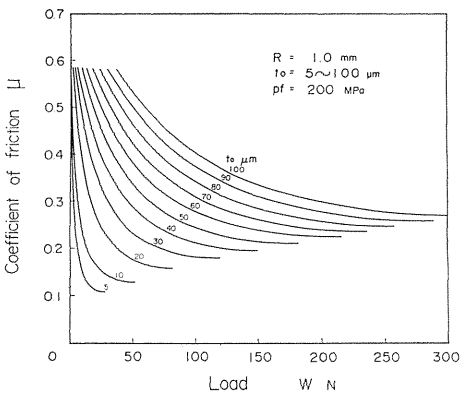

(d) p_f=200 MPa, R=1 mm.

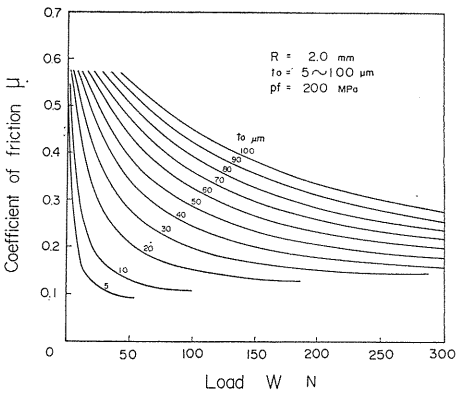

(e) p_f=200 MPa, R=2 mm.

Fig. 21. Effect of film thickness t_0 on coefficient of friction μ.

(c) Effects of deformation resistance p_f of surface film

Figure 22 shows the calculated result of the coefficient of friction when the

deformation resistance p_f of the film is varied. As can be seen in the figure, with the increase of p_f, the coefficient of friction becomes slightly greater and tends to decrease more slowly. When the deformation resistance p_f is large, the penetration depth of the protuberance is shallow and the effect of the underlying metal on the film deformation is limited. Accordingly, the pressure generated in the film is rather low. Furthermore, the ploughing effect is remarkable in the film of large deformation resistance. This may be the reason why the characteristic as shown in Fig. 22 is obtained.

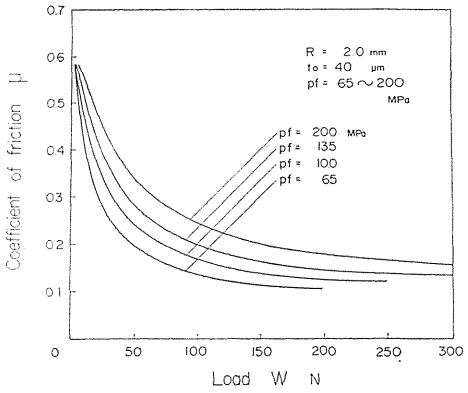

Fig. 22. Effect of deformation resistance p_f of film on coefficient of friction μ.

3. 3. *Comparison between calculated results and experimental results*

In this section, the calculated and experimental results of the coefficient of friction are comared with each other to estimate the mathematical model of film deformation adopted in the analysis. The results obtained using $p_f=100$ MPa are compared with the experimental results of Pb-film. Figure 23 shows the result. As can be seen in the figure, the experimental values are higher than the calculated one. This seems to derive from the piling up of the film ahead of the protuberance. The experimental values are considered to be comparable to the calculated results of

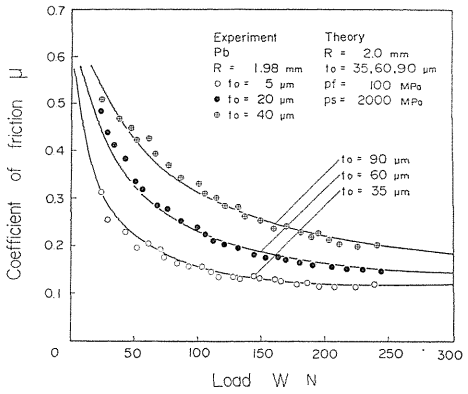

(a) Pb-electroplated film, $R=1.98$ mm.

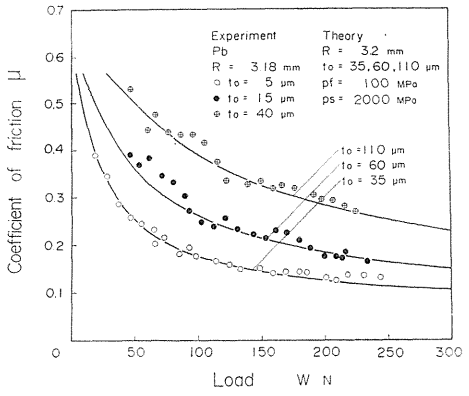

(b) Pb-electroplated film, $R=3.18$ mm.

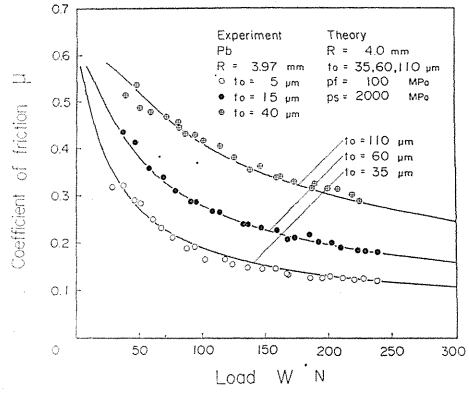

(c) Pb-electroplated film, $R=3.97$ mm.

Fig. 23. Comparison between experimental and calculated values.

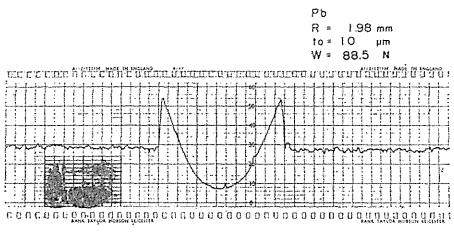

Fig. 24. Profile of friction track.

compensated film thickness, for the effective film thickness is increased by the height of the piled up film. The height of the piled up film, i. e., frictional track, is measured by a surface roughness meter, and an example is shown in Fig. 24. It is seen from the figure that the height of the piled up film is nearly the same order as the film thickness t_0. The piling up shown in Fig. 24 is on the side of the protuberance. The piling up in the front of the protuberance may be higher than that on the side. The degree of agreement between the calculated and experimental values may be improved by considering this effect of the piled up film[12].

So, it can be considered that the calculation of the friction characteristics is qualitatively justified from the experimental results.

3. 4. Concluding remarks on analysis of friction between a single protuberance and surface

Analytical investigation of the evaluation of the coefficient of friction is made in order to clarify the mechanism of the load dependency of friction, and to clarify the effects of the surface film on the friction characteristics. The pressure distribution between a protuberance and the subsurface are clarified, and the coefficient of friction is calculated on the basis of the plane strain model of the deformation of the metal film. As a result, it is confirmed that the characteristic of the coefficient of friction arises from the extremely high pressure generated in the film. The effects of protuberance radius, thickness and deformation resistance of surface film are clarified. The calculated coefficient of friction agrees fairly well with the experimental value, if allowance is made for the influence of the piled up film which is produced in front of the sliding protuberance, in the evaluation of the film thickness.

4. Interference Effect of Soft Metal Film Deformation between Two Protuberances

4. 1. Experiments on friction between soft metal film and two protuberance indentor

4. 1. 1. Experimental apparatus and method

The friction force is measured when indentors having a single protuberance or two protuberances are pressed against the electroplated surface of a rotating disc under a calibrated load. The apparatus used is the same as that used in the single protuberance experiment.

An electroplated disc is attached to the chuck of a lathe and rotated at a slow speed (20mm/sec). The disc material is 0.35% carbon steel electroplated by Pb-alloy (Pb: 95%, Sn: 5%). The indentor is pressed against the electroplated surface, and two components of force acting on the indentor are measured by an annular

dynamometer adhered strain gauges.

To clarify the interference effect induced by a plastic flow of soft metal film, the frictional coefficient is measured not only in the indentor having a single protuberance but also in the indentor having two protuberances located closely to one another. An example oftwo-protuberance indentor is shown in Fig. 25. The protuberances ($R=1$ mm) are made of bearing steel.

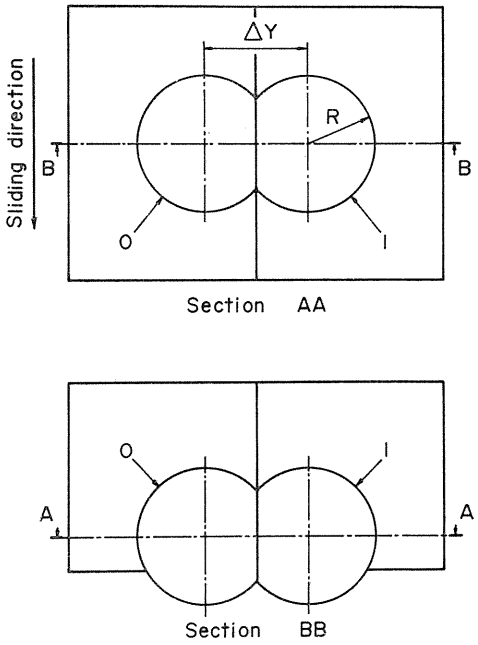

Fig. 25. Two-protuberance indentor.

4. 1. 2. Experimental results

Experimental examples of the relation between applied load W and the coefficient of friction μ are shown in Fig. 26. The experimental results with a single protuberance are plotted by duplicating the normal load W, in order to simplify comparison with the two-protuberance indentor result. There is a distance of $\Delta Y=0.8$ mm between the centers of each protuberance in the two-protuberance indentor in the orthogonal direction to the sliding. The protuberance height in the

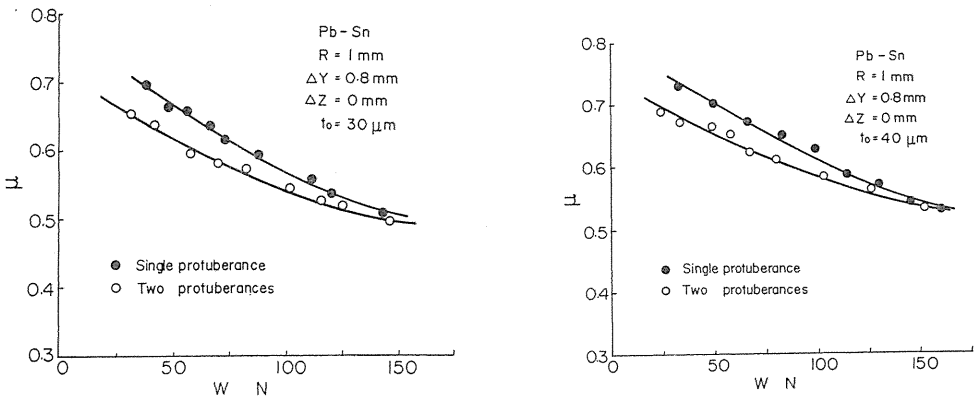

(a) $t_0=30\,\mu$m. (b) $t_0=40\,\mu$m.

Fig. 26. Relation between coefficient of friction μ and normal load W.

film thickness direction is the same ($\Delta Z=0$ mm). Figure 26(a) gives the results with the film thickness $t_0=30\,\mu$m, and Fig. 26(b) with $t_0=40\,\mu$m.

From these experimental results, the following features of interest are obvious.

i) The load dependency in coefficient of friction μ is recognized in cases with either one or two protuberances, and the coefficient of friction μ decreases with

the increase of the applied load.

ii) The coefficient of friction μ of two-protuberance indentor, where the interference effect of plastic film flow exists, is lower than that of single-protuberance indentor.

iii) The difference between single-protuberance indentor and two-protuberance indentor is more remarkable in the light load.

The influence of the interference induced by the plastic film flow and the mechanism that yields the above mentioned friction charactersitics are theoretically investigated in the following section.

4. 2. Calculation of coefficient of friction considering interference effect of plastic film flow

The calculation process for the coefficient of friction and the mechanism yielding the load dependency have already been explained for the single-protuberance indentor[10]. Thus, only the calculation for the case of a two-protuberance indentor is explained in detail here.

4. 2. 1. General idea of interference effect and plastic flow line

The general idea of the interference effect in two-protuberance indentor is clarified by extending the idea of plastic flow in a single-protuberance indentor. Then, the calculation process of the coefficient of friction is given on the basis of this general idea.

Figure 27, which is the same as Fig. 15, shows the contact model of the single protuberance and surface. When the protuberance moves in the arrow direction, the surface film under the leading face of the protuberance will be compressed between the leading face of the sphere and the underlying metal, and forced to flow

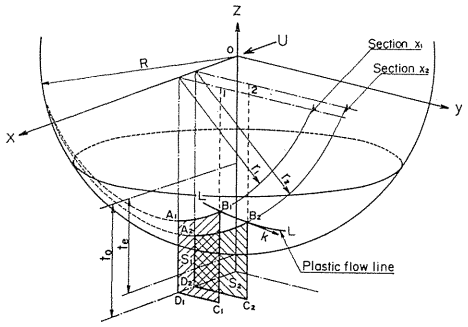

Fig. 27. Plastic flow of metal film between spherical protuberance and underlying metal.

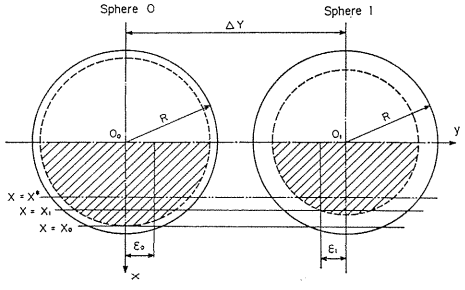

Fig. 28. Arrangement of two-protuberance indentor (top view).

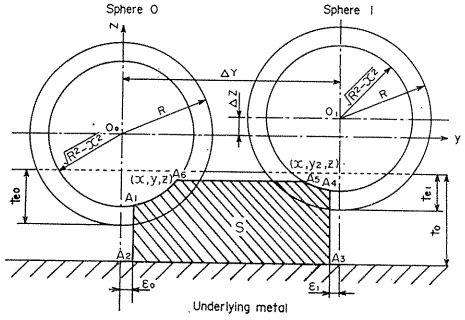

Fig. 29. Arrangement of two-protuberance indentor (front view) and deformation of soft metal film under interference effect.

to both sides. Applying the volume conservation low, plastic flow line LL on the protuberance is obtained in the single-protuberance indentor. This idea is extended to the two-protuberance indentor.

Figures 28 and 29 show the contact of the two protuberance indentor at the soft metal film. In the figures, the adjacent two protuberances are located at intervals of ΔZ, ΔY, in the film thickness direction and in the direction orthogonal to the sliding, respectively. Figure 28 gives a top view and Fig. 29 a front view. The hatched portion in Fig. 28 is the contacting area of protuberances and surface. The lower protuberance is termed "Sphere 0" and the upper one "Sphere 1" hereinafter.

Taking the center O_0 of the spere 0 as the origin, x-axis is determined in the direction of sliding, and z-axis is perpendicular to the contacting surface. Then, y-axis is determind in the direction perpendicular to both x- and z-axis.

Now, the film put between two protuberances cannot flow freely in y direction, because the film deformation in that part is placed under restraint. This phenomenon is the so-called interference effect induced by plastic film flow. For example, the film pushed to the right by Sphere 0 cannot move freely owing to Sphere 1. As a result, the contact pressure occurring in the deformed film may be higher than in the case of a single protuberance. The same fact may be observed in the film pushed to the left by Sphere 1.

The bifurcation of film flow where the film flow divides into two directions shifts from the line of intersection between x-z plane and sphere surface, under the influence of the interference effect. The contact of film and sphere protuberance initiates at the leading front 1 in Fig. 30. This leading front is also a bifurcation of film flow. When the deformation of film becomes large and the interference effect becomes remarkable, the bifurcation on Sphere 0 shifts inside, so that the bifurcation approaches Sphere 1, and the bifurcation line is the curve 1 ~2 in Fig. 30. However, the exact determination of bifurcation is very difficult and the calculation of frictional characteristics becomes complex. Hence, the bifurcations on both spheres are represented as the intersecting lines between the protuberance surface and the plane parallel to x-axis, in the undermentioned analysis. The lines indicated by ε_0 and ε_1 in Figs. 28, 29 show the approximate bifurcations. The locations (ε_0, ε_1) of the appoximate bifurcations are determined so that the contact pressure distribution

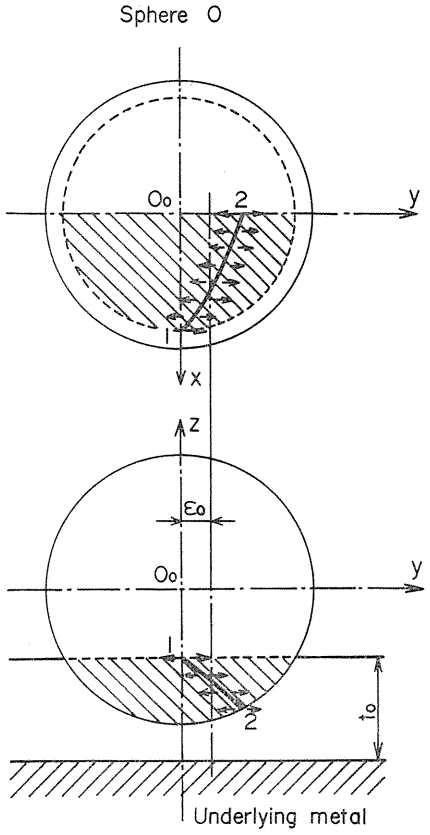

Fig. 30. Location of bifurcation in film flow direction.

on both sides of bifurcation is smoothly maitained.

By arranging the bifurcation in this simple manner, the interference effect does not appear at the outside of the bifurcations of each protuberance and at the inner part which satisfies the relation $x_1 \leqq x \leqq x_0$ $[x_1 = \sqrt{t_{e1}(2R - t_{e1}) - \varepsilon_0{}^2}]$ on Sphere 0.

4. 2. 2. Plastic flow line

The plastic flow line of surface film is calculated from the condition of volume conservation[10]. This condition is simplified to the constant cross-sectional area condition of deformed film, by the assumption of deformation under the plane strain state. As an example, the plastic flow line of surface film will be obtained at the inner part of the bifurcation, $x_1 \leqq x \leqq x_0$, as follows. The same method adopted at the single-protuberance indentor[10]can be applied to this case.

The cross-sectional area S of the configuration $[A_1A_2A_3A_4]$ in Fig. 31 is expressed as follows, by putting the coordinate of the point A_4 as (x, y, z).

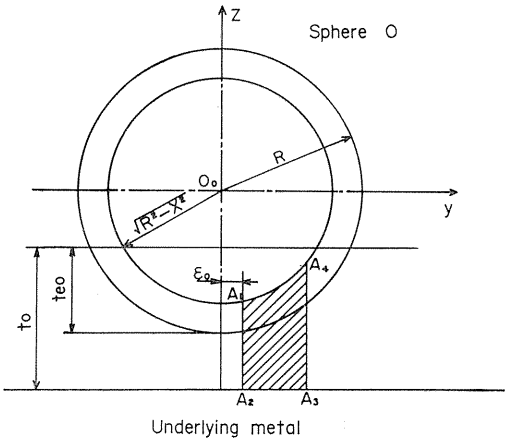

Fig. 31. Soft metal film deformation on non-interference effect side.

$$S(x, y, z) = (R + t_0 - t_{e0})(y - \varepsilon_0) + \int_{\varepsilon_0}^{y} z\, dy$$
$$= S_0 \tag{26}$$

where R, t_0, t_{e0} indicate the protuberance radius, film thickness and penetration depth of Sphere 0, respectively. From the above mentioned condition, the area S_0 shown by equation (26) is constant when measured along the plastic flow line.

Next, the configuration $[A_1A_2A_3A_4A_5A_6]$ in Fig. 29, which is enclosed by two protuberances and underlying metal, must be noteworthy when the plastic flow line is obtained at the inner part of two bifurcations, and the interference effect exists. The cross-sectional area S of the configuration $[A_1A_2A_3A_4A_5A_6]$ is obtained as follows, putting the coordinates of the point A_6 and A_5 as (x, y, z) and (x, y_2, z), respectively.

$$S(x, y, z) = (R + t_0 - t_{e0})(\Delta Y - \varepsilon_0 - \varepsilon_1) + (y_2 - y)z$$
$$+ \int_{\varepsilon_0}^{y} z\, dy + \int_{y_2}^{\Delta Y - \varepsilon_1} z\, dy$$
$$= S_0 \tag{27}$$

It is quite natural in the case of the interference effect of film flow that the area indicated by equation (27) is constant along the plastic flow line on Sphere 0.

The plastic flow line described on Sphere 0 by surface film deformation is expressed as follows, from equations (26) and (27).

$$\left.\begin{aligned} f_1 &= S(x,\ y,\ z) - S_0 = 0 \\ g_1 &= x^2 + y^2 + z^2 - R^2 = 0 \end{aligned}\right\} \tag{28}$$

The plastic flow line on Sphere 1 can be obtained in the same manner.

The directional cosines of the tangent at a given point $(x,\ y,\ z)$ on the plastic flow line [equation (28)] are given as follows:

$$\left.\begin{aligned} l &= \frac{x^*}{\sqrt{x^{*2} + y^{*2} + z^{*2}}} \\ m &= \frac{y^*}{\sqrt{x^{*2} + y^{*2} + z^{*2}}} \\ n &= \frac{z^*}{\sqrt{x^{*2} + y^{*2} + z^{*2}}} \end{aligned}\right\} \tag{29}$$

When the interference effect does not exist, the expressions of x^*, y^*, z^* are:

$$\left.\begin{aligned} x^* &= 2z(R + t_0 - t_{e0} - \sqrt{R^2 - x^2 - y^2}) \\ y^* &= -2xy\left(\sin^{-1}\frac{y}{\sqrt{R^2 - x^2}} - \sin^{-1}\frac{\varepsilon_0}{\sqrt{R^2 - x^2}}\right) \\ z^* &= 2xy\left(\sin^{-1}\frac{y}{\sqrt{R^2 - x^2}} - \sin^{-1}\frac{\varepsilon_0}{\sqrt{R^2 - x^2}}\right) \\ &\quad -2x(R + t_0 - t_{e0} - \sqrt{R^2 - x^2 - y^2}) \end{aligned}\right\} \tag{30}$$

And when the interference effect exists,

$$\left.\begin{aligned} x^* &= -2y(y_2 - y) \\ y^* &= 2x(y_2 - y) - 2xy\left(\sin^{-1}\frac{y}{\sqrt{R^2 - x^2}} - \sin^{-1}\frac{\varepsilon_0}{\sqrt{R^2 - x^2}}\right. \\ &\quad \left. + \sin^{-1}\frac{\Delta Y - y_2}{\sqrt{R^2 - x^2}} - \sin^{-1}\frac{\varepsilon_1}{\sqrt{R^2 - x^2}}\right) \\ z^* &= 2xy\left(\sin^{-1}\frac{y}{\sqrt{R^2 - x^2}} - \sin^{-1}\frac{\varepsilon_0}{\sqrt{R^2 - x^2}}\right. \\ &\quad \left. + \sin^{-1}\frac{\Delta Y - y_2}{\sqrt{R^2 - x^2}} - \sin^{-1}\frac{\varepsilon_1}{\sqrt{R^2 - x^2}}\right) \end{aligned}\right\} \tag{31}$$

Considering that the shearing strength k_f of the film acts along the plastic flow line, the x, y and z components of the shearing stress are represented by the following respective equations.

$$\left.\begin{aligned} k_x &= k_f l \\ k_y &= k_f m \\ k_z &= k_f n \end{aligned}\right\} \tag{32}$$

4. 2. 3. Pressure distribution

The pressure distributions on the protuberances are obtained using the equations of equilibrium and yield condition of soft metal film. In the compression of soft metal film under plane strain between upper and lower rigid surfaces, as shown in Fig. 32, the equation of equilibrium in the y direction is as follows, in the coordinate systems located on each protuberance sphere.

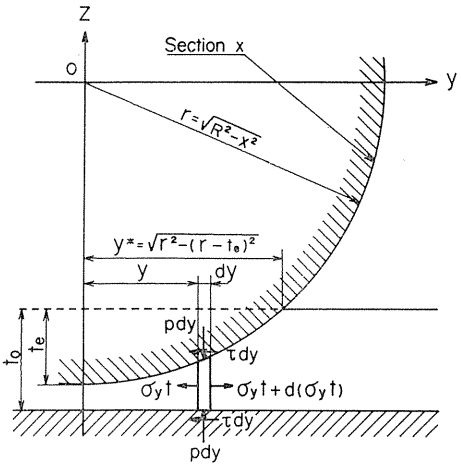

Fig. 32. Compression deformation under plane strain.

$$\frac{d\sigma_y}{dy}=\frac{2\tau}{t}-\frac{\sigma_y}{t}\frac{dt}{dy} \tag{33}$$

where t represents the effective film thickness, and is written as follows:

$$t=R+t_0-t_e-\sqrt{R^2-x^2-y^2} \tag{34}$$

By putting $t_e=t_{e0}$ (penetration depth of Sphere 0) in equation (34), equation (33) corresponds to Sphere 0. And by putting $t_e=t_{e1}$ (penetration depth of Sphere 1), equation (33) corresponds to Sphere 1.

The yield condition of the infinitely small element in Fig. 32 is

$$\sigma_y+p=2k_f \tag{35}$$

From equation (32), the relation $\tau=mk_f$ is obtained. By taking this relation into consideration, it follows from equations (33)~(35) that

$$p=\frac{2k_f}{t^2}\left\{\int\left(-mt+\frac{2yt}{\sqrt{R^2-x^2-y^2}}\right)dy+C\right\} \tag{36}$$

The integral constant C in equation (36) is determined so that $p=p_f$ (deformation resistance of surface film) at the point of $y=\sqrt{2Rt_e-t_e^2-x^2}$.

The pressure distribution p does not exceed the deformation resistance p_s of the underlying metal. When the calculated value of p by equation (36) exceeds p_s, the pressure p is determined as $p=p_s$.

4. 2. 4. Coefficient of friction

From the previous preparation, the coefficient of friction can be calculated

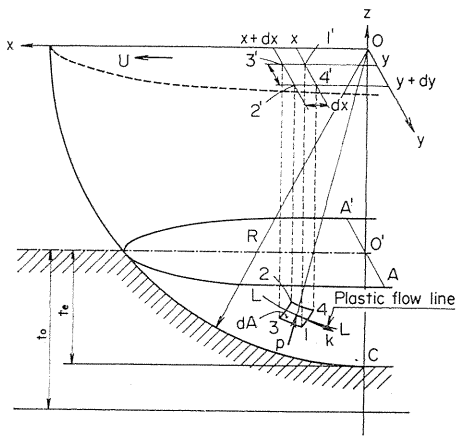

Fig. 33. Stress distribution on spherical protuberance.

when the two-protuberance indentor is pressed against the soft metal surface under the prescribed normal load W.

In Fig. 33 showing the spherical protuberance, the area dA of spherical surface element 1234 is written as follows:

$$dA=\frac{R\,dx\,dy}{\sqrt{R^2-x^2-y^2}} \tag{37}$$

Pressure p acts perpendicularly to this surface element, and shearing deformation stress of the film k_f acts along the plastic flow lines. The force components dF_i, dW_i in x and z directions acting on the small surface element 1234 are written as follows:

$$\left.\begin{aligned} dF_i&=(\bar{\lambda}p+lk_f)\,dA\\ dW_i&=(\bar{\nu}p+nk_f)\,dA \end{aligned}\right\} \tag{38}$$

where $\bar{\lambda}=x/R$ and $\bar{\nu}=z/R$ are direction cosines of the normal of the sphere. In equation (38), the conditions which represent $i=0$, $i=1$ correspond to Sphere 0 and Sphere 1, respectively.

The frictional force F_i and the normal force W_i can be represented as

$$\left.\begin{aligned} W_i&=\int_0^{\sqrt{2Rt_e-t_e^2}}dx\int_{-\sqrt{2Rt_e-t_e^2-x^2}}^{\sqrt{2Rt_e-t_e^2-x^2}}\frac{(\bar{\nu}p+nk_f)R}{\sqrt{R^2-x^2-y^2}}dy\\ F_i&=\int_0^{\sqrt{2Rt_e-t_e^2}}dx\int_{-\sqrt{2Rt_e-t_e^2-x^2}}^{\sqrt{2Rt_e-t_e^2-x^2}}\frac{(\bar{\lambda}p+lk_f)R}{\sqrt{R^2-x^2-y^2}}dy \end{aligned}\right\} \tag{39}$$

Therefore, the coefficient of friction μ can be obtained by

$$\mu=\frac{F_0+F_1}{W_0+W_1} \tag{40}$$

The coefficient of friction of single-protuberance indentor can be obtained with almost the same calculation method by neglecting the interference effect of plastic film flow and locating the bifurcation of the film flow at the intersecting line between the protuberance surface and the plane through the protuberance center.

4. 3. Calculation results and considerations

4. 3. 1. Location of bifurcation and contact pressure distribution

In a single-protuberance indentor, the surface film flow direction divides right and left at the boundary of the intersecting line between the sphere and the vertical plane including the sphere center. In the two-protuberance indentor, on the other hand, the correct determination of the bifurcation location is very important in the estimation of the interference effect of the plastic film flow on the frictional characteristics, even if the configuration of the bifurcation is simplified as stated in section 4. 2. 1. In the present section, the determination process of the simplified bifurcation is explained. The bifurcation location is determined by considering the contact pressure distribution. In the calculation, the deformation pressure p_s, p_f of underlying metal and the electroplated surface film obtained from the hardness test are used; $p_s=1960$ MPa and $p_f=98$ MPa. The shearing strength k_f of the surface film is estimated from the measured value of the coefficient of friction shown in Fig. 26; $k_f=80$ MPa.

Next, calculations are carried out for the two-protuberance indentor with symmetrical arragement of each protuberance ($\Delta x=\Delta z=0$) and compared with the calculation for a single-protuberance indentor.

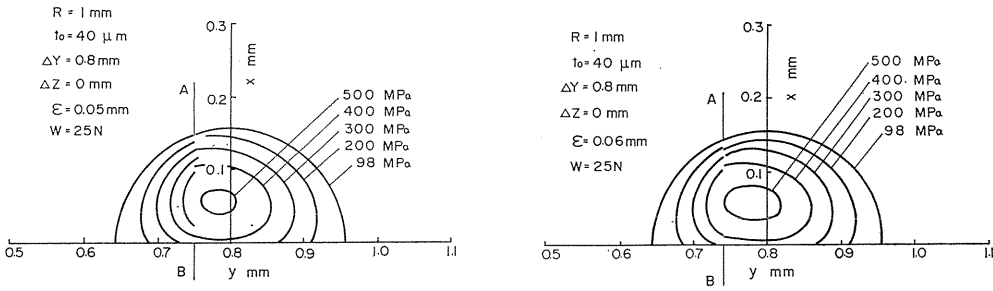

(a) $\varepsilon=0.05$ mm. (b) $\varepsilon=0.06$ mm.

Fig. 34. Relation between bifurcation location and contact pressure distribution.

An example of the calculated contact pressure distribution for the two-protuberance indentor is shown in Fig. 34, varying the location of the bifurcation. The indicated distribution is of the protuberance sphere 1, and that of the protuberance sphere 0 is symmetric with respect to the center line. As recognized in the figure, the contact pressure distribution is greatly changed by the location ε of the bifurcation measured from the protuberance center. In the figure, the contact pressure distribution on both sides of the bifurcation continues smoothly, when

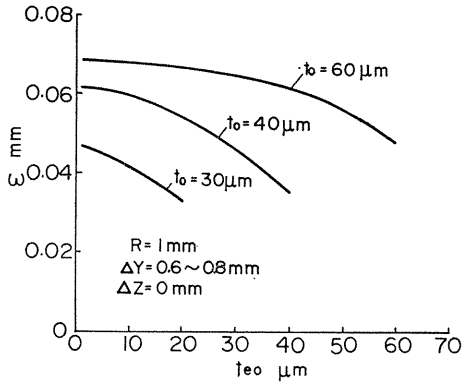

Fig. 35. Location of bifurcation.

$\varepsilon = 0.06$ mm.

The right location of the bifurcation is obtained from the smooth continuation of contact pressure distribution. The bifurcation of the two-protuberance indentor of symmetrical arrangement is shown in Fig. 35. The location of bifurcation is changed by the film thickness t_0, normal load W (i. e., penetration depth t_{e0} of indentor). The deviation from the protuberance center of the bifurcation is large when an indentor is pressed against a thick soft metal film by a light load.

4. 3. 2. Effect of interference on frictional characteristics

The interference effect on the frictional characteristic of soft metal surface is investigated in this section. The coefficients of friction μ for the single- and two-protuberance indentor with symmetrical arrangement are compared with each other in Fig. 36. The normal load acting on the single-protuberance indentor is doubled in the figure to compare with the two-protucerance indentor, as in the experiment. The coefficient of friction μ of the two-protuberance indentor is smaller than that of single-protuberance indentor. The load dependency of the coefficient of friction μ is remarkable in the two-protuberance indentor owing to the interference effect. This tendency is clear in the light load region. The difference in the two-protuberance indentor and single-protuberance indentor decreases with the increase of normal load. These characteristics recognized in the calculation are qualitatively in agreement with those in the experiments. Hence, it is clarified that the interference effect of plastic

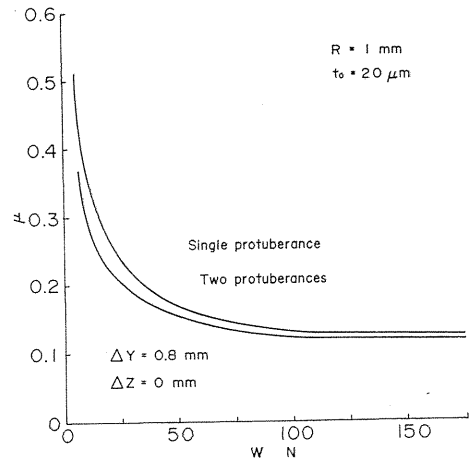

(a) $t_0 = 20\ \mu$m.

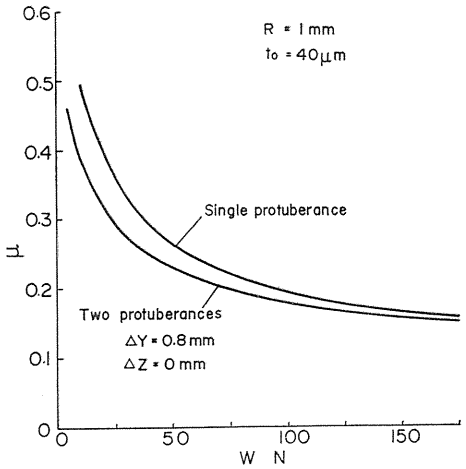

(b) $t_0 = 40\ \mu$m.

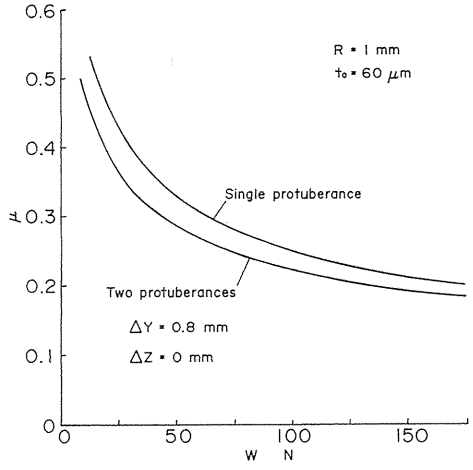

(c) $t_0 = 60\ \mu$m.

Fig. 36. Relation between coefficient of friction μ and normal load W.

film flow can be well explained by the model shown in Fig. 29.

The coefficient of friction μ increases with the increase of film thickness t_0 in the case of two-protuberance indentor, too, as recognized in Fig. 36. Furthermore, it is recognized in the same figure that the friction difference between single- and two-protuberance indentor is large when thicker film thickness is used.

4. 3. 3. Discussion and consideration

The reason for the difference in the frictional characteristic yields owing to the interference effect is discussed from the viewpoints of contact pressure distribution and plastic film flow on the protuberance surface. The next discussions concern only for two applied normal loads. One is the light load case (W=25N) where the difference of the coefficient of friction is large and the other is the large load case (W=150 N) where the difference is small.

Figures 37~39 show the plastic flow line and contact pressure distribution in W=25 N for both types of indentor. Figures 37 and 38 are top and side views of the plastic flow line. The contact pressure distribution has already been indicated in Fig. 34 (b). The plastic flow line in the two-protuberance indentor is shown only for Sphere 1. On the left side of the bifurcation AB, the interference effect is induced; thus soft metal film flows to the left and runs against the film flow by Sphere 0. At the right side of AB, no such interference effect is induced. The flow line in Fig. 38 (a) corresponds to that at the left side of AB in Fig. 37 (a). From these figures showing the plastic flow line, the following features are noted.

In the single-protuberance indentor, soft metal film flows almost parallel to the sliding direction of the indentor in the entire contact area. On the other hand,

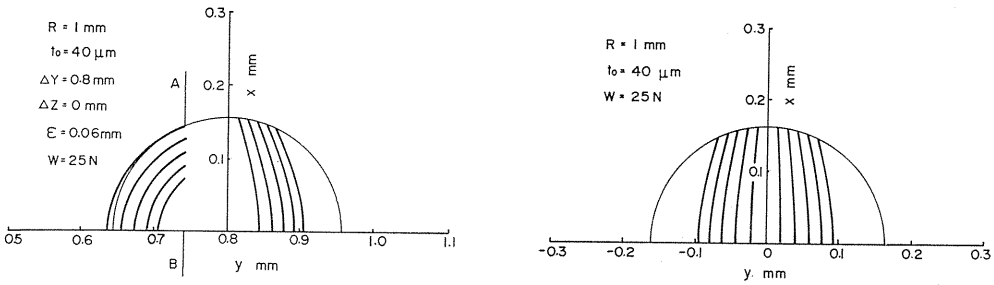

(a) Two-protuberance indentor. (b) Single-protuberance indentor.

Fig. 37. Plastic flow lines (top view in case of W=25 N).

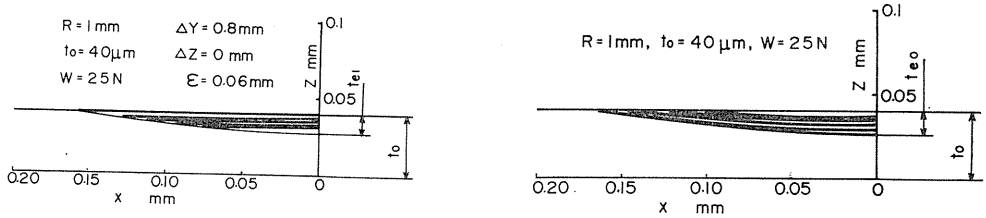

(a) Two-protuberance indentor. (b) Single-protuberance indentor.

Fig. 38. Plastic flow lines (side view in case of W=25 N).

in the two-protuberance indentor, the soft metal film flow spreads sideways owing to the interference effect. This tendency is remarkable at the left side of the bifurcation AB, which is kept between the two protuberances. Accordingly, the soft metal film in the two-protuberance indentor flows upwards in the left side of bifurcation, in comparison with the flow line in the single-protuberance indentor [see Fig. 38 (a) and Fig. 38 (b)]. On the right side of the bifurcation, the plastic flow line spreads slightly sideways as seen in Fig. 37 (b). The soft metal film also flows upwards slightly there, possibly increasing the force pushing up the indentor normally.

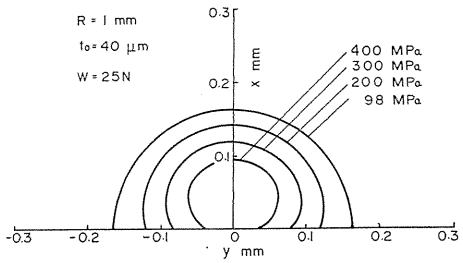

Fig. 39. Contact pressure distribution (single-protuberance indentor, W=25N).

Taking these factors into consideration, Fig. 39 and Fig. 34 showing the contact pressure distribution are compared to each other and examined. Remarkably higher contact pressure is generated in the two-protuberance indentor by the interference effect, than in the single-protuberance indentor. The contact area supporting the normal load (W=25 N) is small in the two-protuberance indentor. Hence, the frictional resistance acting on the protuberances and the coefficient of friction become smaller in the two-protuberance indentor than in the single-protuberance indentor.

The plastic flow lines and contact pressure distribution are shown in Figs. 40～42, for a large normal load (W=150 N), where the interference effect on the frictional characteristic is not clear. The configurations of the plastic flow line described by the flowing film on the protuberance have the same tendency as seen in Figs. 37, 38. However, the depth of indentor penetration is great and the generated contact pressure is high owing to the large applied load. The area where the contact pressure reaches the deformation pressure p_s of the underlying metal is wide in both indentors. The contact pressure distributions of both indentors are similar. The difference between the contact area of both indentors decreases in a large applied load. These are the reasons why the difference of frictional characteristic in single- and two-protuberance indentor decreases in large applied load conditions.

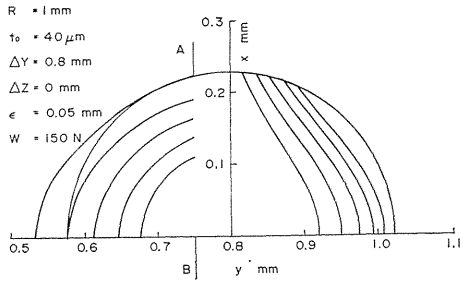

(a) Two-protuberance indentor.

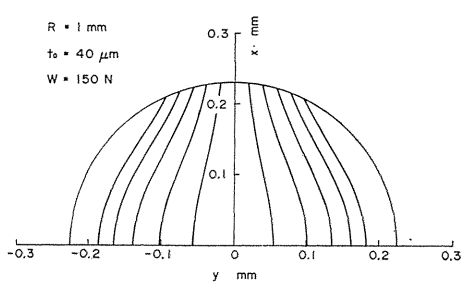

(b) Single-protuberance indentor.

Fig. 40. Plastic flow lines (top view in case of W=150 N).

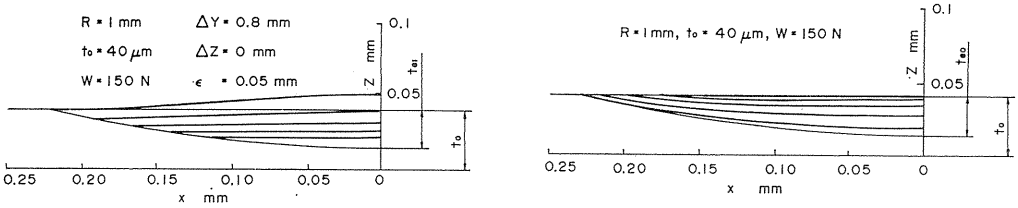

(a) Two-protuberance indentor. (b) Single-protuberance indentor.

Fig. 41. Plastic flow lines (side view in case of W=150 N).

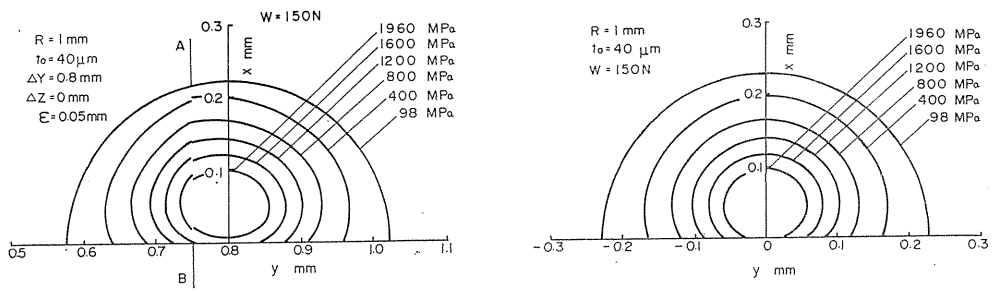

(a) Two-protuberance indentor. (b) Single-protuberance indentor.

Fig. 42. Contact pressure distribution (W=150 N).

It may be concluded from the above consideration that the interference effect of plastic film flow can be estimated from the configuration of the plastic flow line described by the film flow and the contact pressure distribution generated between the indentor and the soft metal film.

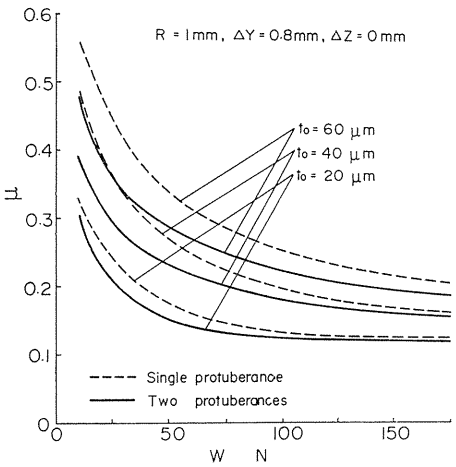

Fig. 43. Relation between coefficient of friction μ and normal load W (calculational result when film thickness t_0 is varied).

The load dependency of the coefficient of friction is shown in Fig. 43 for various film thickness, using the same indentors used in Fig. 36. The coefficient of friction increases with the film thickness. The load dependency characteristics recognized are identical with each other. That is to say, the coefficient of friction decreases by the interference effect of plastic film flow, and the difference of friction between two-protuberance and single-protuberance indentor is remarkable in light load conditions.

Here, the occurring mechanism of such frictional features are discussed. Figure 44 shows the relations between contact area, mean contact pressure and normal load. These parameters are good criteria for the contact state. The contact area increases with the film thickness t_0. The

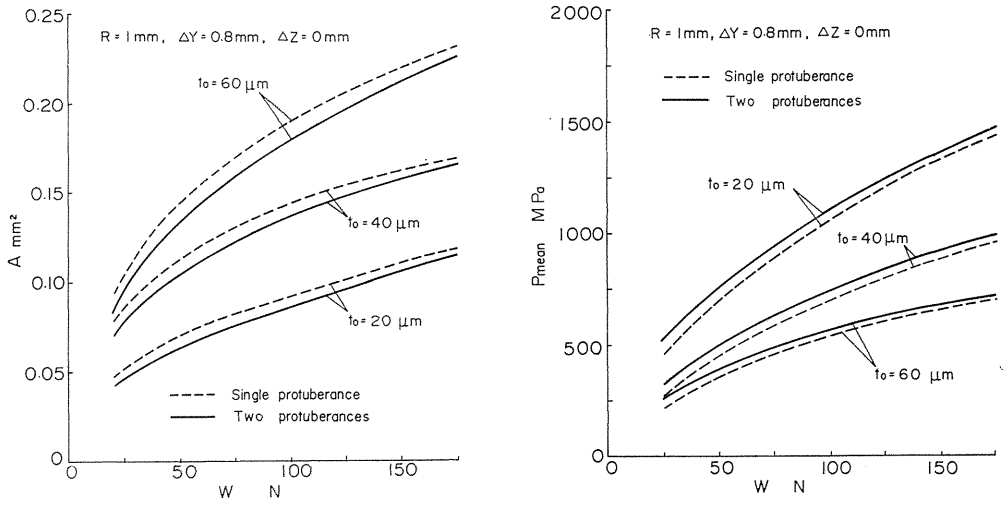

(a) Contact area. (b) Mean contact pressure.

Fig. 44. Contacting state of indentor and soft metal film when film thickness t_0 is varied.

mean contact pressure of two-protuberance indentor is higher than that of the single-protuberance indentor, and the contact area decreases, too. The difference of these features between two-protuberance and single-protuberance indentor is remarkable in light load conditions. These tendencies correspond to the frictional tendency shown in Fig. 43. The considerations for $t_0=40\mu$m (Figs. 37, 38) are therefore valid for other film thicknesses.

From the above discussions, it can be ascertained that the interference effect acts mainly on the contact pressure distribution generated in the contact area of the indentor and the soft metal film, and the coefficient of friction decreases. This is a general rule in an arbitrary contacting condition of indentor and film.

4. 4. Concluding remarks on interference effect of soft metal film deformation between two protuberances

The interference effect induced by a plastic flow of soft metal film on the frictional properties is discussed in the contact of the indentor with two spherical model protuberances located close to one another and a soft metal film, to obtain basic knowledge on the contact problem of a surface composed of many micro asperities. In the theoretical examination, an interference model of plastic film flow within adjacent protuberances is proposed, and a calculated friction characteristic based on this model is compared with the characteristic of the single-protuberance indentor.

As a result, the calculated coefficient of friction agrees qualitatively with the experimental one. Thus, proposed interference model is ascertained to be reasonable. The coefficient of friction decreases by the interference effect induced in plastic film flow. This result can be explained through the configuration of plastic flow line described on the protuberance sphere and the contact pressure distribution.

Some differences between the calculated coefficient of friction and the theoretical are noted. This may be due to the fact that the characteristic values of

soft metal film used in the calculation does not adequately represent the nature of the film used in the experiment. The nature of the film needs more investigation in the state in which it is attached to the hard underlying metal.

5. Conclusion

First, the frictional properties in the contact between single hard protuberance and the metal surface covered by soft thin metal film are examined experimentally. The protuberance used in the experiment is a hard steel ball which simulates asperities on many engineering surfaces. The load dependency of the coefficient of friction and the effects of thickness and hardness of the film on the friction are clarified. The simple empirical expression of friction which represents the effect of the film properties is presented, considering the deformation mechanism of the surface film. Analytical investigation of the evaluation of the coefficient of friction is made to clarify the mechanism of the load dependency of friction, which was obtained in the experiment, and also to ascertain the effects of the surface film on the friction characteristic. The plastic flow of the soft metal film betweeen a protuberance and the surface is presumed, and the pressure distribution originating from the side flow is calculated on the basis of the plasticity theory. The effects on the coefficient of friction of the load, the thickness and hardness of the film, and the radius of the protuberance, are examined. As a result, it is clarified that the load dependency of friction arises from the extremely high pressure distribution generated in the film.

The real engineering surfaces are composed of many micro asperities. So, the interference effect of plastic film flow may excert some influence on the frictional characteristics. Then, to obtain some knowledges on the interference effect, the frictional characteristic is examined, when a two-protuberance-indentor is slid on a surface covered by electroplated soft metal film. The result is compared with that of a single-protuberance indentor. The coefficient of friction in a two-protuberance indentor, where the interference effect exists, is lower than in a single-protuberance indentor, where the interference effect does not. This fact can well be explained with the configuration of plastic flow line on protuberances described by deforming soft metal film, and the corresponding contact pressure distribution between protuberances and a surface.

The application of this interference model proposed here to the real engineering surface is now examined experimentally and theoretically, and will be reported next.

References

1) Bowden, F. P., and Tabor, D., "The Friction and Lubrication of Solids," 1964, Oxford.
2) Tsuya, Y., and Takagi, R., "Lubricating Properties of Lead Films on Copper," Wear, Vol. 7, 1964, p. 131.
3) Bowers, R. C., and Zisman, W. A., "Pressure Effects on the Friction Coefficient of Thin-Film Solid Lubricants," Journal of Applied Physics, Vol. 39, No. 12, Nov. 1968, p. 5385.

4) Finkin, E. F., "A Theory for the Effects of Film Thickness and Normal Load in the Friction of Thin Films," Trans. ASME, Ser. F, Vol. 91, No. 3, July, 1969, p. 551.
5) Rabinowitcz, E., "Variation of Friction and Wear of Solid Lubricant Film Thickness," ASLE Transactions, Vol. 10, No. 1. Jan. 1967, p. 1.
6) Kato, S., et. al., "Some Considerations on Characteristics of Static Friction of Machine Tool Slideway," Trans. ASME, Ser. F, Vol. 94, No. 3, July 1972, p. 234.
7) Kato, S., et. al., "Frictional Properties of a Surface Covered With a Soft Metal Film-Part 1: Experiments on Friction Between a Single Protuberance and a Surface," Trans. ASME, Journal of Lubrication Technology, Vol. 103, No. 2, April 1981, p. 236.
8) Lowen, E. G., and Cook, N. H., "Metal Cutting Measurements and Their Interpretation," Experimental Stress Analysis, Vol. 13, Part I, 1956, p. 57.
9) Tsukizoe, T., and Hisakado, T., "The Influence of Surface Roughness on the Mechanism of Friction" Trans. ASME, Ser. F, Vol. 92, No. 2, April 1970, p. 264.
10) Kato, S., et. al., "Frictional Properties of a Surface Covered with a Soft Metal Film-Part 2: Analysis of Friction Between a Single Protuberance and a Surface," Trans. ASME, Journal of Lubrication Technology, Vol. 104, No. 1, January 1982, p. 39.
11) Hill, R., "The Mathematical Theory of Plasticity," Oxford at the Clarendon Press, 1950.
12) Tsukizoe, T., and Sakamoto, T., "Mechanism of Dry Friction (Part 4, On the Geometrical Shape of Scratch)," Trans. JSME, Vol. 40, No. 332, April 1974, p. 1179.